Atlantic Geology
Journal of the Atlantic Geoscience Society
Revue de la Société Géoscientifique de l'Atlantique

U-Pb geochronology and geochemistry from the northeastern New River belt, southern New Brunswick, Canada: significance of the Almond Road Group to the Ganderian platformal margin

Susan C. Johnson, Gregory R. Dunning and Brent V. Miller

Volume 54, 2018

URI: https://id.erudit.org/iderudit/1055414ar
DOI: https://doi.org/10.4138/atlgeol.2018.005

See table of contents

Publisher(s)

Atlantic Geoscience Society

ISSN

0843-5561 (print)
1718-7885 (digital)

Explore this journal

Cite this article

Johnson, S., Dunning, G. & Miller, B. (2018). U-Pb geochronology and geochemistry from the northeastern New River belt, southern New Brunswick, Canada: significance of the Almond Road Group to the Ganderian platformal margin. *Atlantic Geology*, *54*, 147–170. https://doi.org/10.4138/atlgeol.2018.005

Article abstract

The Almond Road Group in the northeastern New River belt comprises two formations: the basal Snider Mountain Formation contains orthoquartzite, feldspathic quartzite, and quartzite pebble conglomerate; the gradationally overlying Ketchum Brook Formation is composed of feldspathic sandstone, laminated dark siltstone and shale, overlain by mafic lithic tuffs and basaltic flows. The Almond Road Group overlies latest Ediacaran to earliest Cambrian (early Fortunian) pyroclastic, volcaniclastic, and epiclastic rocks of the Belleisle Bay Group. Based in part on this relationship, the Almond Road Group was thought to be Early Cambrian, although an upper age limit had never been determined. A U–Pb (zircon) age of 475 ± 2 Ma for the West Scotch Settlement porphyry, a small felsic hypabyssal intrusion emplaced into the Ketchum Brook Formation, demonstrates that the Almond Road Group is no younger than Early Ordovician (early Floian) age. Its age is further constrained by LA ICP-MS detrital zircon data from a basal quartzite in the Snider Mountain Formation. Results show a dominant peak in the Ediacaran (ca. 575 Ma), with the youngest coherent cluster of ages at ca. 530–520 Ma. Together these data support a Cambrian age for the quartz-rich Almond Road Group and its platformal relationship to Ganderia.

U–Pb geochronology and geochemistry from the northeastern New River belt, southern New Brunswick, Canada: significance of the Almond Road Group to the Ganderian platformal margin

Susan C. Johnson[1]*, Gregory R. Dunning[2], and Brent V. Miller[3]

1. New Brunswick Department of Energy and Resource Development, Geological Survey Branch, Sussex, New Brunswick E4E 7H7, Canada
2. Department of Earth Sciences, Memorial University of Newfoundland, St. John's, Newfoundland and Labrador A1B 3X5, Canada
3. Department of Geology and Geophysics, Texas A & M University, College Station, Texas 77843-3115, USA

*Corresponding author <susan.johnson@gnb.ca>

Date received: 02 January 2018 ¶ Date accepted: 17 February 2018

ABSTRACT

The Almond Road Group in the northeastern New River belt comprises two formations: the basal Snider Mountain Formation contains orthoquartzite, feldspathic quartzite, and quartzite pebble conglomerate; the gradationally overlying Ketchum Brook Formation is composed of feldspathic sandstone, laminated dark siltstone and shale, overlain by mafic lithic tuffs and basaltic flows. The Almond Road Group overlies latest Ediacaran to earliest Cambrian (early Fortunian) pyroclastic, volcaniclastic, and epiclastic rocks of the Belleisle Bay Group. Based in part on this relationship, the Almond Road Group was thought to be Early Cambrian, although an upper age limit had never been determined. A U–Pb (zircon) age of 475 ± 2 Ma for the West Scotch Settlement porphyry, a small felsic hypabyssal intrusion emplaced into the Ketchum Brook Formation, demonstrates that the Almond Road Group is no younger than Early Ordovician (early Floian) age. Its age is further constrained by LA ICP-MS detrital zircon data from a basal quartzite in the Snider Mountain Formation. Results show a dominant peak in the Ediacaran (ca. 575 Ma), with the youngest coherent cluster of ages at ca. 530–520 Ma. Together these data support a Cambrian age for the quartz-rich Almond Road Group and its platformal relationship to Ganderia.

RÉSUMÉ

Le groupe d'Almond Road, dans la ceinture nord-est de New River, comporte deux formations : la formation basale de Snider Mountain, qui contient de l'orthoquartzite, du quartzite feldspathique et un conglomérat de cailloux de quartz; la formation de Ketchum Brook, progressivement superposée et composée de grès feldspathique, de siltite feuilleté foncé et de schiste superposé de tuf lithique mafique et de coulées basaltiques. Le groupe d'Almond Road repose sur des roches pyroclastiques, volcanoclastiques et épiclastiques allant de l'Édiacarien tardif au Cambrien précoce (Fortunien précoce) du Groupe de Belleisle Bay. En raison en partie de cette relation, on estimait que le groupe d'Almond Road datait du Cambrien précoce, quoique la limite d'âge supérieure n'ait pas été déterminée. Une datation U-Pb (zircon) de 475 ± 2 Ma pour le porphyre de West Scotch Settlement, une petite intrusion felsique hypabyssale à position fixe de la formation de Ketchum Brook, montre que le groupe d'Almond Road ne date pas d'avant l'Ordovicien précoce (Floien précoce). Les données tirées du zircon détritique d'un échantillon de quartzite basal de la formation de Snider Mountain par spectromètre de masse à plasma inductif à ablation par laser restreignent l'âge davantage. Les résultats indiquent un sommet dominant pendant l'Édiacarien (environ 575 Ma), la plus jeune grappe d'âges cohérente étant d'environ 530 à 520 Ma. Mises ensemble, ces données appuient l'âge du Cambrien pour le groupe d'Almond Road riche en quartz, de même que sa relation avec les plates-formes du Gandérien.

[Traduit par la redaction]

doi: 10.4138/atlgeol.2018.005

INTRODUCTION AND REGIONAL GEOLOGICAL SETTING

The New River belt (NRB) is the westernmost of three Proterozoic lithotectonic belts within the broader northeastern Appalachian orogen in southern New Brunswick (Fig. 1). These Proterozoic belts represent the peri-Gondwanan microcontinents of Ganderia and Avalonia (Barr and White 1996b; Fyffe *et al.* 2009, 2011; Johnson *et al.* 2012; van Staal and Barr 2012; Barr *et al.* 2014a, b). The easternmost Proterozoic rocks are in the Caledonia belt, which is the only belt in southern New Brunswick assigned to Avalonia (Barr and White 1996a). The Brookville and New River belts are interpreted to be part of Ganderia; these rocks form the basement to younger, Early Paleozoic arcs (Penobscot and Popelogan-Victoria) and back-arc complexes (Tetagouche-Exploits) exposed in south-central, central and northern New Brunswick, and central Newfoundland (van Staal *et al.* 2003; Wilson 2003; Hibbard *et al.* 2006; Zagorevski *et al.* 2010; Fyffe *et al.* 2011). The succession of Proterozoic rocks in the NRB and Caledonia belt are similar in that both contain Ediacaran volcanic and comagmatic rocks that formed in two separate pulses, one around ~ 625 Ma and a later one at ~ 555 Ma, and both lacking rocks representative of the ~70 million year hiatus. The Brookville belt that now separates the NRB and Caledonia belt shares only the later Ediacaran magmatic episode (~ 555 Ma) and includes an older ~ 650 Ma carbonate platform signifying a Late Cryogenian passive margin believed to have developed separately from Avalonia (Barr *et al.* 2014c).

The NRB belt extends from islands in Head Harbour Passage in the Bay of Fundy and trends northeast to the headland west of Maces Bay on mainland southern New Brunswick where it continues inland for a distance of over 160 kms (Figs. 1, 2). The NRB is truncated to the east by the Belleisle Fault, which separates it from the Early Silurian volcanic rocks of the Kingston Group (Figs. 1). The Kingston Group, and partially time-equivalent Mascarene

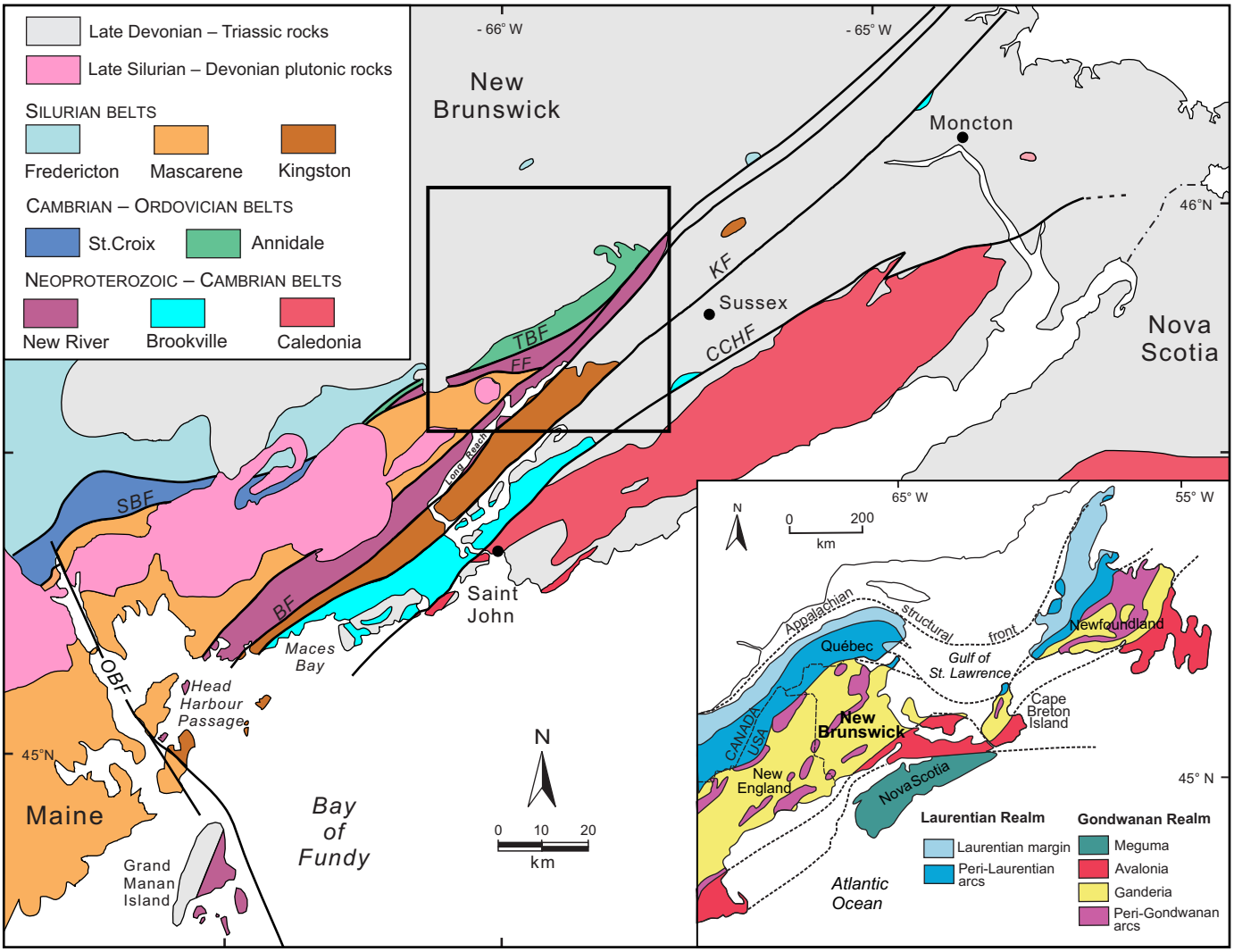

Figure 1. Major geological subdivisions in southern New Brunswick showing the distribution of Neoproterozoic, Cambrian to Ordovician and Silurian belts. Area outlined in black is location of Figure 2. Inset map shows major tectonic elements of the northeastern Appalachians in New England and Atlantic Canada. List of fault abbreviations: BF – Belleisle; CCHF – Caledonia-Clover Hill; FF – Fanning Brook KF – Kennebecasis; OBF – Oak Bay; SBF – Sawyer Brook TBF – Taylors Brook.

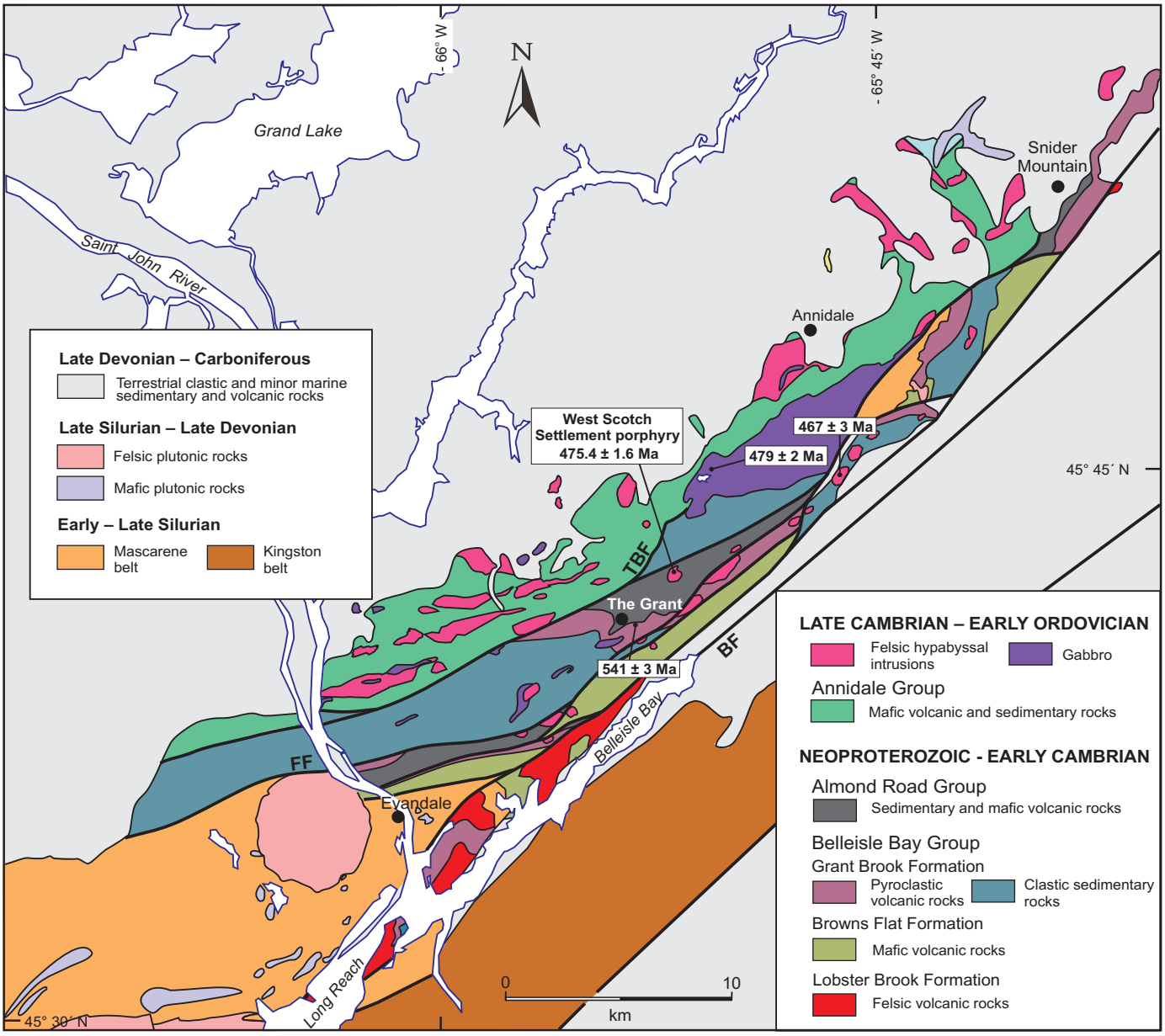

Figure 2. Simplified geological map of the northeastern New River belt and Annidale belt. Numbers in boxes are U–Pb (zircon) crystallization ages from Johnson *et al.* 2012 and this study. Fault abbreviations as in Figure 1.

Group that in New Brunswick is preserved within the NRB, represent an Early Silurian arc and back-arc complex, respectively, which were built on NRB Proterozoic basement and the overlying Early Paleozoic arc/back-arc complexes during an episode of northwest-directed (NW-dipping) subduction (Fyffe *et al.*1999; Barr *et al.* 2002). To the northwest, the NRB is juxtaposed against Cambrian to Ordovician rocks of the St. Croix and Annidale belts along the Sawyer Brook and Taylor Brook faults, respectively. To the southwest, the NRB trends toward coastal Maine where the Proterozoic rocks are likely to underlie the Cambrian Ellsworth Schist and Castine Volcanics of the Ellsworth belt (Fyffe and Fricker 1987; Schulz *et al.* 2008; Fyffe *et al.* 2009).

The NRB is typified by (1) Neoproterozoic arc-related, comagmatic volcanic and plutonic rocks of early Ediacaran (ca. 629–622 Ma) and late Ediacaran (ca. 555–551 Ma) age (Johnson and McLeod 1996; Johnson 2001; Johnson and Barr 2004), (2) latest Ediacaran–earliest Cambrian (ca. 540 Ma) relatively shallow marine to subaerial pyroclastic volcanic and sedimentary rocks of the Belleisle Bay Group and (3) post-540 Ma cover of Cambrian marine sedimentary and minor volcanic rocks. The Cambrian cover rocks occur in three separate structural panels that subparallel the northeasterly strike of the belt, with the most inboard panel being closest to the Kingston belt, and the most outboard panel closest to the Annidale belt (Johnson 2001; Johnson *et al.* 2009; Fyffe *et al.* 2011). From farthest inboard to farthest outboard these younger Cambrian rocks are divided into the Saint John, Almond Road, and Ellsworth groups, respectively. All three sequences are either directly un-

derlain by the Belleisle Bay Group, as is the case with the Almond Road Group and Saint John Group in the Long Reach area, or linked to the Belleisle Bay Group by means of detrital zircon as is the case for the Ellsworth Group (Fyffe *et al.* 2009). Although the quartz-rich Almond Road Group was not previously dated, it was considered to be approximately the same age as the Matthews Lake Formation of the Ellsworth Group and Glen Falls Formation of the Saint John Group (e.g., Fyffe *et al.* 2011; fig. 4). The age of orthoquartzite and quartzose sandstone in the Matthews Lake Formation, the lower unit of the Ellsworth Group in the NRB, is constrained by earliest Cambrian detrital zircon in the basal beds (Fyffe *et al.* 2009) and a ca. 514 Ma U–Pb age for the overlying volcanic rocks (McLeod *et al.* 2003). The Early Cambrian age for orthoquartzite in the Glen Falls Formation, in the lower part of the Saint John Group, is also fairly well-constrained by dated ash beds, macrofossils, and acritarch assemblages in overlying and underlying formations (e.g., Tanoli and Pickerill 1988; Landing *et al.* 2008; Palacios *et al.* 2011, 2017), but the age of the Almond Road Group was poorly constrained until now.

We report new U–Pb (zircon) data that provide upper and lower age limits on the Almond Road Group. The maximum age of the basal quartzite in the group is Early Cambrian (late Fortunian), based on the youngest concordant detrital zircon population at ca. 530 Ma. The minimum age is Early Ordovician (early Floian) based on a U–Pb age of ca. 475 Ma for the cross-cutting West Scotch Settlement porphyry. Together these data support previous interpretations that Early Cambrian quartz-rich strata in the Ellsworth, Almond Road, and Saint John groups once formed a continuous, distal to proximal, Ganderian sandstone facies spanning all three structural panels of the NRB (Johnson *et al.* 2009; Fyffe *et al.* 2011) and may have extended across the Avalonian Caledonia belt as well.

STRATIGRAPHY OF THE NORTHEASTERN NEW RIVER BELT

The northeastern NRB is defined here as the structural panel between the Belleisle and Taylor Brook faults, west of Belleisle Bay and northeast of the Long Reach (Fig. 2). The Taylor Brook Fault shows evidence that it was initially a thrust fault that has been cut by a late steep structure that presently defines a large part of the boundary between the NRB and Annidale belt. With the exception of small, local fault-bounded units, the Silurian Mascarene Group is restricted to the area south of the Fanning Brook Fault, along the complexly faulted southern margin of the NRB in this area (Fig. 2). This lack of Silurian cover may be due to the oblique east-northeast-trend of the Fanning Brook Fault, which cuts across the regional northeast structural trend exposing older rocks on its north side (Fig. 1). Consequently this structural panel is the only one in which the basement rocks on the north side of the Mascarene basin are exposed.

The stratigraphic succession in the northeastern NRB is composed of the Almond Road Group and underlying Belleisle Bay Group. The Belleisle Bay Group in this area comprises two formations; the Browns Flat and Grant Brook formations. The Browns Flat Formation is not dated, but the overlying and in part laterally equivalent Grant Brook Formation yielded a U–Pb zircon age of 541 ± 3 Ma age for a slightly reworked intermediate to felsic tuff. Previous attempts to date the Grant Brook Formation yielded a maximum age of 542 ± 9 Ma (unpublished data from T. Krogh in Johnson *et al.* 2009), which is considered to be close to the depositional age based on the more recent age data. Historically the vast majority of rocks now included in the Belleisle Bay and Almond Road groups were assigned to the Silurian Mascarene Group (e.g., McCutcheon and Ruitenberg 1987). However, a pre-Silurian age for the Grant Brook Formation is demonstrated by the intense hornfelsing of the unit near the contact with the Early Ordovician (479 ± 2 Ma) Stewarton Gabbro (Johnson *et al.* 2009, 2012) and the Middle Ordovician (467 ± 3 Ma) age obtained for the cross-cutting Bull Moose Hill porphyry (Johnson *et al.* 2012).

Almond Road Group

The Almond Road Group is divided into the Snider Mountain Formation and overlying Ketchum Brook Formation (Johnson *et al.* 2009). The group is exposed north of Evandale on the east side of the Saint John River and on Spragg, Taylors and Ketchum brooks near The Grant (Fig. 2). It is also exposed farther northeast on Snider Mountain where it is overstepped by Carboniferous rocks of the Maritimes Basin.

Snider Mountain Formation

The Snider Mountain Formation is named after a section of rocks on Snider Mountain north of Sussex (Figs. 1, 2). On the Snider Mountain Road the formation is composed of white to grey orthoquartzite and intraformational quartzite-pebble-rich conglomerate that appears to be concordantly underlain by pink feldspathic sandstone and pink to reddish arkosic pebble conglomerate of the Grant Brook Formation. There is a gap of a few metres in the exposure, but the quartzite unit contains rare red siltstone clasts presumed to be from the Grant Brook Formation. Along strike to the northeast on Beatty Brook, similar pink feldspathic sandstone and pebbly arkosic conglomerate are succeeded down-section by thick-bedded, volcaniclastic rocks, reworked tuffs, and various pyroclastic volcanic rocks that are also part of the Grant Brook Formation.

The Snider Mountain Formation is also well-exposed on a tributary of Jones Brook where is crosses the Almond Road, east of the Saint John River (Fig. 3). Here it is composed of thick-bedded (65–70 cm), white, granular orthoquartzite (Fig. 4), intercalated with thin-bedded, fine-grained, light grey, feldspathic quartzite. The lack of pebble conglomerate at this location may indicate that these strata were depos-

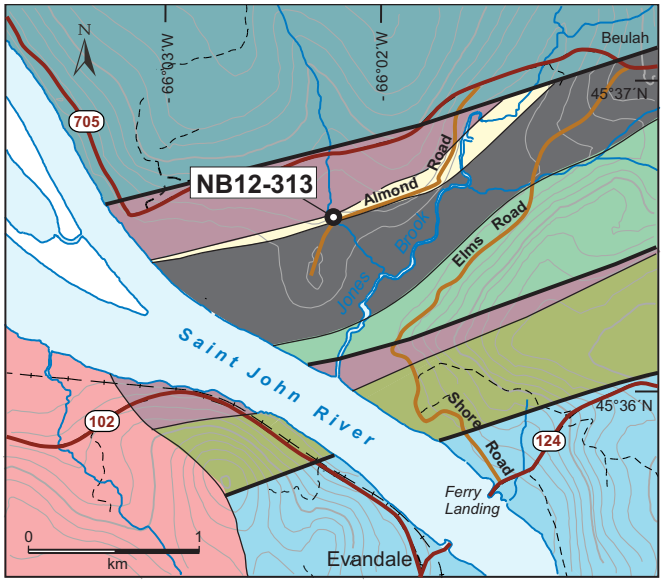

Figure 3. Detailed geology of the Almond Road Group type area showing location of sample NB12-313 collected for U–Pb dating.

ited farther offshore than those exposed at the type section on Snider Mountain. The quartzite unit is about 20 metres thick and is separated from underlying purple and greyish green ash tuffs of the Grant Brook Formation by a small (< 5 m) concealed zone. The orthoquartzite is succeeded upsection to the south by dark grey siltstone interbedded with fine- to medium-grained, quartz-rich, feldspathic sandstone of the overlying Ketchum Brook Formation on the south side of Almond Road (it should be noted that much of the outcrop on the south side of the road is now covered by rip-rap during 2017 road improvements). Orthoquartzite from this locality on the north side of Almond Road was sampled for detrital zircon. Results are described below in the Geochronology section.

Figure 4. Field photograph of Snider Mountain Formation thick-bedded orthoquartzite at the dated locality on tributary of Jones Brook, north of Almond Road.

Ketchum Brook Formation

The Ketchum Brook Formation is characterized by the exposures on Spragg, Taylors and Ketchum brooks (Fig.5), and in the Beulah area and south of Almond Road (Fig. 3). The formation is divided into a lower sedimentary member and an upper mafic volcanic member. The sedimentary rocks comprise light grey, thin- to thick-bedded (5–50 cms), fine- to medium-grained, slightly micaceous, quartz-rich, feldspathic sandstone intercalated with dark grey to black laminated siltstone and shale and minor thinly-laminated, light green siltstone, and shale. Near Beulah on a west-flowing tributary of Jones Brook the dark shale dominates and it is interbedded with rare limestone and calcareous siltstone with well-developed cone-in-cone structures. Cone-in-cone structures are diagenetic concretionary features resembling horn corals. Younging direction determined from the cone-in-cone structures show that the clastic rocks are overlain by the mafic volcanic rocks. Intercalations of dark shale and mafic tuff can be viewed on Highway 705 southeast of Beulah (Fig. 3). The mafic volcanic member comprises light grey, commonly bleached, highly amygdaloidal basalt flows and grey green, basaltic lithic tuff dominated by coarse mafic volcanic lapilli.

On Ketchum Brook south of the second bridge on Elm Flat Road only the lower sedimentary member is exposed and here is composed of thick-bedded (40–50 cm), light grey, medium-grained, micaceous, quartz-rich feldspathic sandstone, with thinner (2 cm) interbeds of finer grained, light grey quartzose sandstone and thinly laminated, light green siltstone and shale. To the north on Taylors Brook, it grades upwards into interbedded dark grey to black laminated siltstone and light grey, very fine-to medium-grained, micaceous, feldspathic sandstone. Sandstone beds range in thickness from about 2–20 cm. The Ketchum Brook Formation is intruded by a small number of mostly unnamed, felsic and mafic intrusive plugs and rhyolite domes.

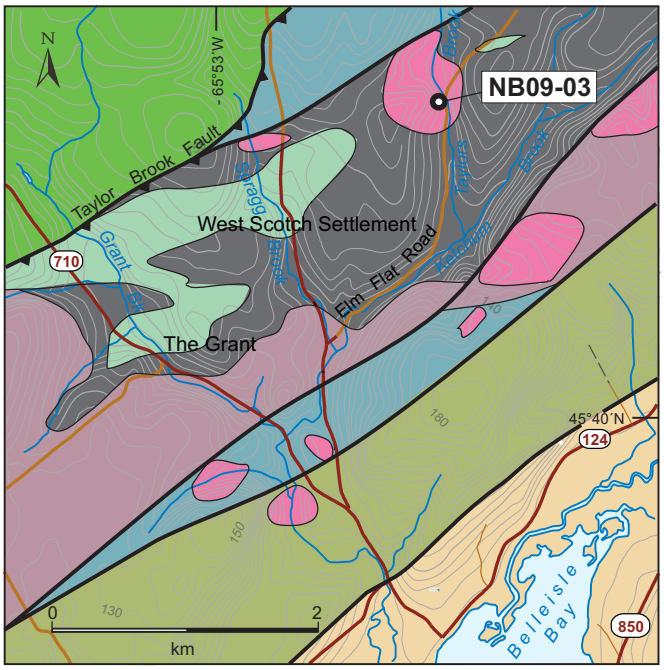

CARBONIFEROUS

Sedimentary rocks

Dated sample location

ORDOVICIAN

West Scotch Settlement porphyry and unnamed hypabyssal felsic intrusions

LATE CAMBRIAN – EARLY ORDOVICIAN

Annidale Group

Mafic volcanic and sedimentary rocks

CAMBRIAN

Almond Road Group

Ketchum Brook Formation: Mafic volcanic rocks

Ketchum Brook Formation: Sedimentary rocks

LATEST NEOPROTEROZOIC - EARLY CAMBRIAN

Belleisle Bay Group

Grant Brook Formation: Pyroclastic volcanic/ epiclastic sedimentary rocks

Browns Flat Formation: Mafic volcanic rocks

Figure 5. Detailed geology of the West Scotch Settlement area showing the location of sample NB09-03.

West Scotch Settlement porphyry

The West Scotch Settlement porphyry is a small, hypabyssal felsic intrusion that is less than 1 kilometre in diameter. The intrusion is exposed on Elm Flat Road approximately 2.4 km north of its junction with the West Scotch Settlement Road and on Taylor Brook where it intrudes the Ketchum Brook Formation (Fig.5). The West Scotch Settlement porphyry has abundant euhedral to anhedral feldspar and quartz phenocrysts in an aphantic matrix. The intrusion exhibits a rusty weathered surface due to the presence of iron-oxide from abundant disseminated pyrite. The feldspar phenocrysts and feldspar in the groundmass are pervasively altered to buff white clay. The intrusion is exposed sporadically along Taylors Brook for about 500 metres north of the junction with the Elm Flat Road, at which point it intrudes dark siltstone and white sandstone of the Ketchum Brook Formation. The intrusion–sediment contact is very irregular and dark sedimentary fragments are incorporated into the intrusion at the contact, which is brecciated and contains quartz veins with pyrite.

GEOCHRONOLOGY

West Scotch Settlement porphyry

Sample NB09-03 (UTM 20T –5063608 N, 277333 E) was collected from outcrop on the west side of Elm Flat Road where it turns and crosses over Taylors Brook (Fig.5).

Analytical methods and results

U–Pb analyses were conducted by Greg Dunning at the Geochronology Laboratory in the Department of Earth Sciences at Memorial University of Newfoundland using chemical abrasion - thermal ionization mass spectrometry (CA-TIMS) methods. The analyses were carried out according to the technique outlined in Sánchez-García *et al.* (2008). The zircons were annealed, and then etched using the Mattinson (2005) technique, which is very effective at eliminating altered portions of zircon that have undergone lead-loss. The ages were calculated using the decay constants recommended by Jaffey *et al.* (1971). The U–Pb isotopic composition is shown in Table 1.

The zircon population in plane light under the picking microscope and the cathodoluminescence images of the representative grains are shown on Figures 6a and 6b. The sample has three concordant points of 3–5 zircon prisms each (Fig. 7). The three points yield $^{206}Pb/^{238}U$ ages as follows: Z1 – 476 ± 3; Z2 – 475.5 ± 2.3; Z3 – 474.6 ± 3 Ma. The weighted average of these at the 95% confidence interval is 475.4 ± 1.6 Ma (MSWD = 0.24) indicating an Early Ordovician (Floian) age for the West Scotch Settlement porphyry.

Snider Mountain Formation

Sample NB12-313 (UTM 19T – 5054899 N, 731021 E) was collected from orthoquartzite outcrop on a tributary of Jones Brook less than 20 metres north of where it crosses the Almond Road (Figs. 3, 4). Detrital zircon from the sample is shown in Figure 8.

Analytical methods

Detrital zircon U-Th-Pb laser-ablation, inductively coupled plasma mass spectrometry (LA-ICPMS) analyses

Table 1. U-Pb isotope composition and age for West Scotch Settlement intrusion (NB09-03).

Fraction	Wt. (mg)[a]	Concentration U (ppm)	Concentration Pb_{rad} (ppm)[b]	Measured Total common Pb (pg)	Measured $^{206}Pb/^{204}Pb$	Corrected atomic ratios[c] $^{208}Pb/^{206}Pb$	$^{206}Pb/^{238}U$	$^{207}Pb/^{235}U$	$^{207}Pb/^{206}Pb$	Age (Ma) $^{206}Pb/^{238}U$	$^{207}Pb/^{235}U$	$^{207}Pb/^{206}Pb$
Z1 5 sml clr euh prm Etch	0.005	604	50.3	6	2611	0.2056	0.07663 ± 48	0.5995 ± 52	0.05675 ± 42	476	477	482
Z2 3 sml clr euh prm Etch	0.003	460	38.6	4	1839	0.2155	0.07655 ± 40	0.5971 ± 32	0.05658 ± 18	475	475	475
Z3 3 sml clr euh prm Etch	0.003	785	66.0	6	1920	0.2223	0.07640 ± 48	0.5976 ± 38	0.05672 ± 16	475	476	481

Z, zircon; 3 and 5 No. of grains in the analysis; clr, clear; euh, euhedral; prm, prism; sml, small; Etch, zircons annealed, then etched with HF; (chemical abrasion of Mattinson 2005); a Weights of grains were estimated, with potential uncertainties of 25%–50% for small samples; b Radiogenic lead; c Atomic ratios corrected for fractionation, spike, laboratory blank of 0.6–2.0 picograms (pg) common lead, and initial common lead at the age of the sample calculated from the model of Stacey and Kramers (1975), and 0.3 pg U blank. 2 σ uncertainties are reported after the ratios and refer to the final digits.

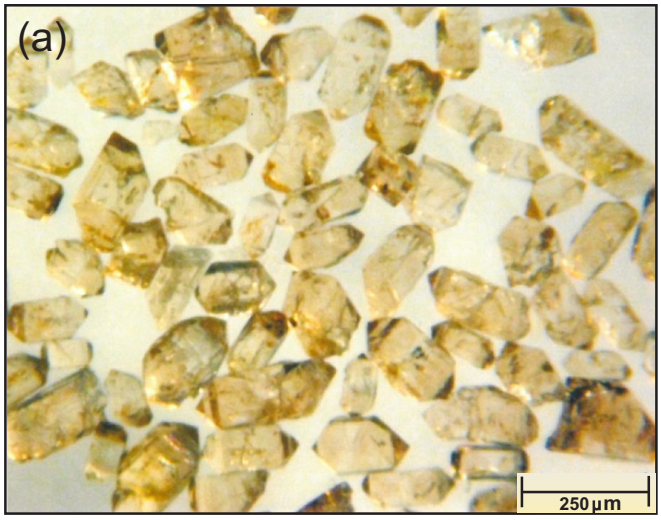

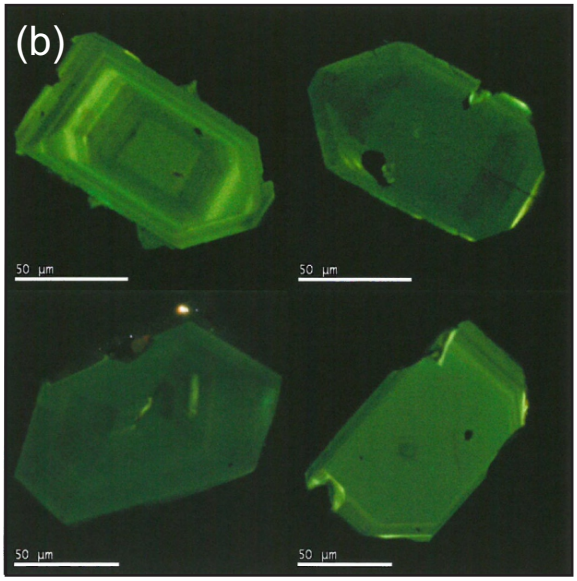

Figure 6. Sample NB09-03 (a) photograph of the zircon population in plane light under the picking microscope and (b) cathodoluminescence images of the representative zircon grains.

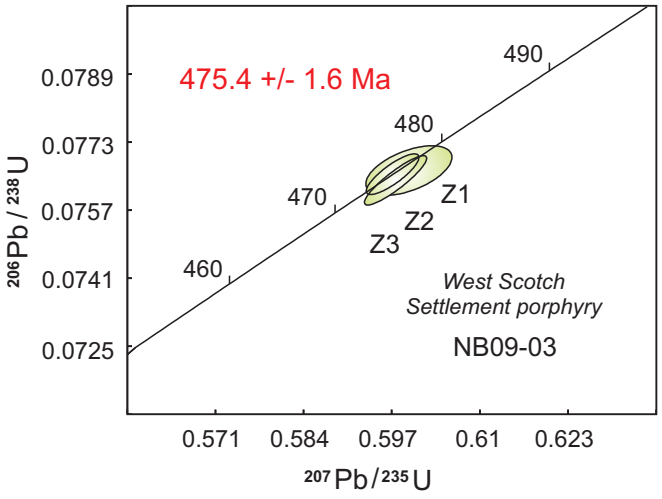

Figure 7. Concordia diagram for NB09-03. Analytical data listed in Table 1.

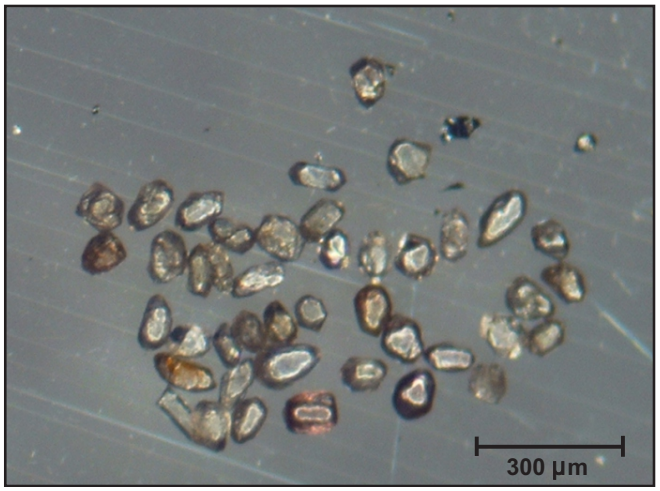

Figure 8. Transmitted light photograph of detrital zircons from sample NB12-313.

were conducted at the Texas A & M University R. Ken Williams Radiogenic Isotope Geosciences Laboratory. Rock samples were crushed and zircon grains concentrated using standard crushing and density separation (jaw and disc crusher, Wilfley table, heavy liquids) methods. Zircon grains were separated from other dense minerals by hand-picking in a petrie dish under a binocular microscope, but no further separation was performed on the bulk zircon aliquot recovered from heavy liquids. The bulk zircon aliquot was piled and quartered repeatedly in the petrie dish to obtain an unbiased (or minimally biased) sub-sample of about 1000 grains. This zircon sub-sample was mounted on double-stick tape and encased in a 2.5cm diameter epoxy disc, along with fragments of NIST 610, NIST 612, one primary reference material (zircon 91500; Wiedenbeck *et al.* (1995) and two secondary reference materials (zircons R33 and FC-1; Black *et al.* 2004; Paces and Miller 1993, respectively). The disk was abraded with 2000 grit sandpaper to expose the interior of zircon grains and polished to 0.25µm on a diamond-suspension lap wheel.

LA-ICPMS analyses were conducted on a Thermo Scientific iCAP RQ quadrupole mass spectrometer running in standard high-sensitivity (STDS) mode connected to an esi/NWR 193nm 4ns pulsed excimer laser system equipped with a two-volume sample cell (TV-2). Instrument settings and run parameters are given in Table 2 and analytical data in Appendix A. Data are reduced using Iolite v. 3.5 (Paton *et al.* 2011) under the U–Pb Geochron4 data reduction scheme (Paton *et al.* 2010). Analysis of the primary reference material, each treated separately as an unknown, indicates an internal analytical reproducibility of U–Pb ages to better than 0.7%. The average accuracy of secondary reference materials (Appendix A) is better than 2.25% (FC-1) and better than 1.5% (R33).

Results

A total of 177 zircon grains were analyzed from sample NB12-313. A gap in dates at around 700 Ma provides a convenient cut-off below which the $^{206}Pb/^{238}U$ dates are preferred and above which the $^{207}Pb/^{206}Pb$ dates are preferred. Of the analyzed grains, 51 were either >10% discordant or were of <10% precision on their preferred U–Pb date. The age spectrum is dominated by a peak centered at about 575 Ma (Fig. 9a). It is important to note that in a detrital suite it is unlikely that these represent a single population of zircon; therefore at least some of the individual analyses that cluster around 575 Ma may actually be younger, within error of the 560–550 Ma volcanic and co-magmatic plutonic rocks now exposed in the NRB. The apparent youngest grain has a $^{206}Pb/^{238}U$ age of 515 ± 5.5 Ma, (Fig. 9b, Appendix A) but it lies within error of a fairly continuous distribution of dates with no clear "cluster" of youngest dates and thus the data do not provide clear evidence for providing a quantifiable maximum age of deposition. The youngest population of zircons yielded a Concordia age of 529.2 ± 3.6 Ma indicating a depositional age of ca. 530 Ma or younger (Fig. 9c).

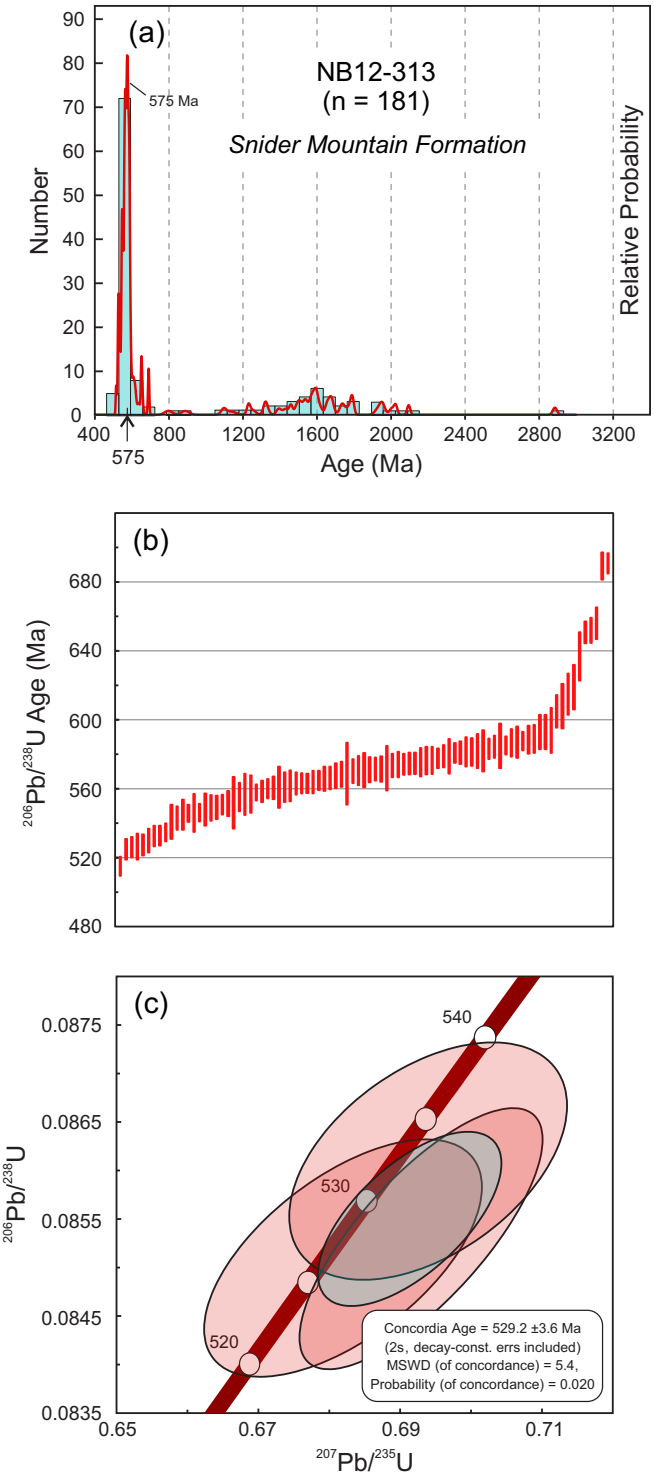

Figure 9. Sample NB12-313 (a) Relative probability plot and histogram and (b) age distribution of the youngest detrital zircons. (c) Concordia plot of the youngest detrital zircon population. Box heights in b are 2σ. Analytical data are listed in Appendix A.

CHEMICAL DATA

A total of 22 samples of mafic to intermediate volcanic rocks were chosen for analysis. The sampled units include the Ketchum Brook Formation in the Almond Road Group (4 samples), and the Grant Brook (12 samples) and Browns Flat (6 samples) formations in the Belleisle Bay Group. The majority of volcanic rocks in the Browns Flat and Ketchum Brook formations are basalt, whereas the composition of the Grant Brook Formation volcanic rocks is mainly andesitic or basaltic andesite (Fig.10a). Three of the analysed samples from the latter formation contained > 63% SiO_2 (Appendix B), although only one of these plots in the rhyolite- dacite field based on immobile trace element ratios (Fig.10a). Immobile trace element ratios were also utilized to determine the magmatic affinity of the volcanic rocks in the northeastern NRB (Fig. 10b). The Th/Yb against Zr/Y bivariate diagram of Ross and Bedard (2009) was chosen as these authors have demonstrated that it is an improvement on Barrett and McLean's (1994, 1999) single ratio diagrams using Zr versus Y, La versus Yb and Th versus Yb, although the data are still somewhat ambiguous. The basalt in the Browns Flat Formation plot almost exclusively in the transitional field, although one sample was clearly calc-alkaline (Fig. 10b). Basalt samples from the Ketchum Brook Formation are similar in that the four samples span the tholeiitic, transitional, and calc-alkaline fields. The one tholeiitic sample in the Ketchum Brook Formation was collected from the same general area as another that plots well into the transitional field but the reason why the trace element ratios are so different is not clear. In contrast, the Grant Brook Formation is clearly calc-alkaline based on Th/Yb and Zr/Y ratios (Fig. 10b).

On N-MORB-normalized trace element spider diagrams all of the samples exhibit depletion in Nb relative to Th or La (Fig. 11) that is typical of arc magmas. The Belleisle Bay Group exhibits three slightly different patterns that correlate directly with the composition of the volcanic rocks. As would be expected the most felsic samples in the Grant Brook Formation show the most pronounced depletion in Ti (Figs. 11b, 11c, and 11d). Basalts from the Browns Flat and Grant Brook formations are similar and lend support to the field evidence that suggests these formations are in part laterally equivalent. The younger Ketchum Brook Formation basalt samples exhibit patterns similar to those in the Belleisle Bay Group and are indistinguishable from them based on trace element patterns alone.

On a tectonic discrimination diagram using high field strength elements such as the Th-Hf-Ta of Wood (1980), all of the volcanic rocks in the Belleisle Bay and Almond Road groups plot in the volcanic arc basalt field (Fig. 12a) and are displaced above the diagonal line representing mid-ocean ridge basalt (MORB) and ocean island basalt (OIB) on the Th/Yb versus Nb/Yb diagram (Fig. 12b) of Pearce (2008), indicating that they interacted with continental crust or were erupted in a supra-subduction zone environment (Pearce and Peate 1995).

Table 2. Analytical Parameters.

laser	esi/NWR 193 nm 4 ns excimer
background/washout	14 s /8 s
laser repetition rate	15 Hz
spot size/shape	30 µm / circle
fluence	3.25 J cm^{-2}
carrier/makeup gas	0.6 l/min He, 0.8 l/min Ar
mass spectrometer	Thermo Scientific iCAP RQ
plasma RF power	1550 W
total duty cycle	195 ms
isotopes measured (dwell times in ms)	^{48}Ti (10), ^{88}Sr (10), ^{96}Zr (2.5), ^{179}Hf (2.5), ^{202}Hg (10), ^{204}Pb (20), ^{206}Pb (20), ^{207}Pb (50), ^{208}Pb (10), ^{232}Th (10), ^{235}U (20), ^{238}U (10), ^{232}Th^{16}O (10), ^{238}U^{16}O (10)

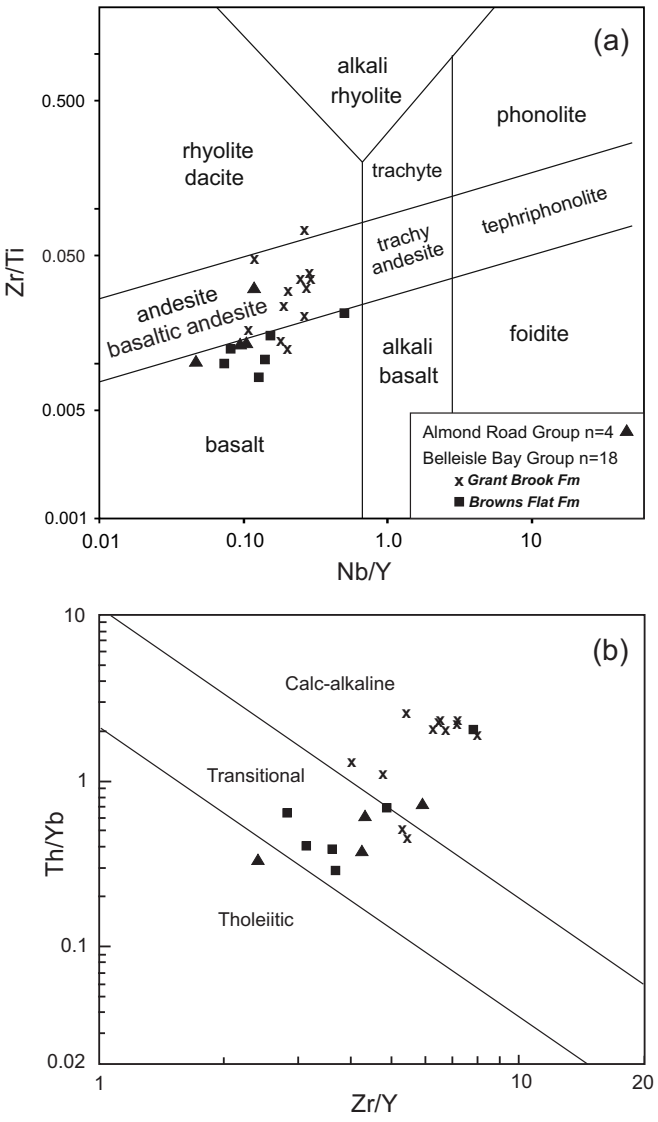

Figure 10. Zr/Ti vs Nb/Y classification diagram for volcanic rocks in the Almond Road and Belleisle Bay groups from Pearce (1996) after Winchester and Floyd (1977).

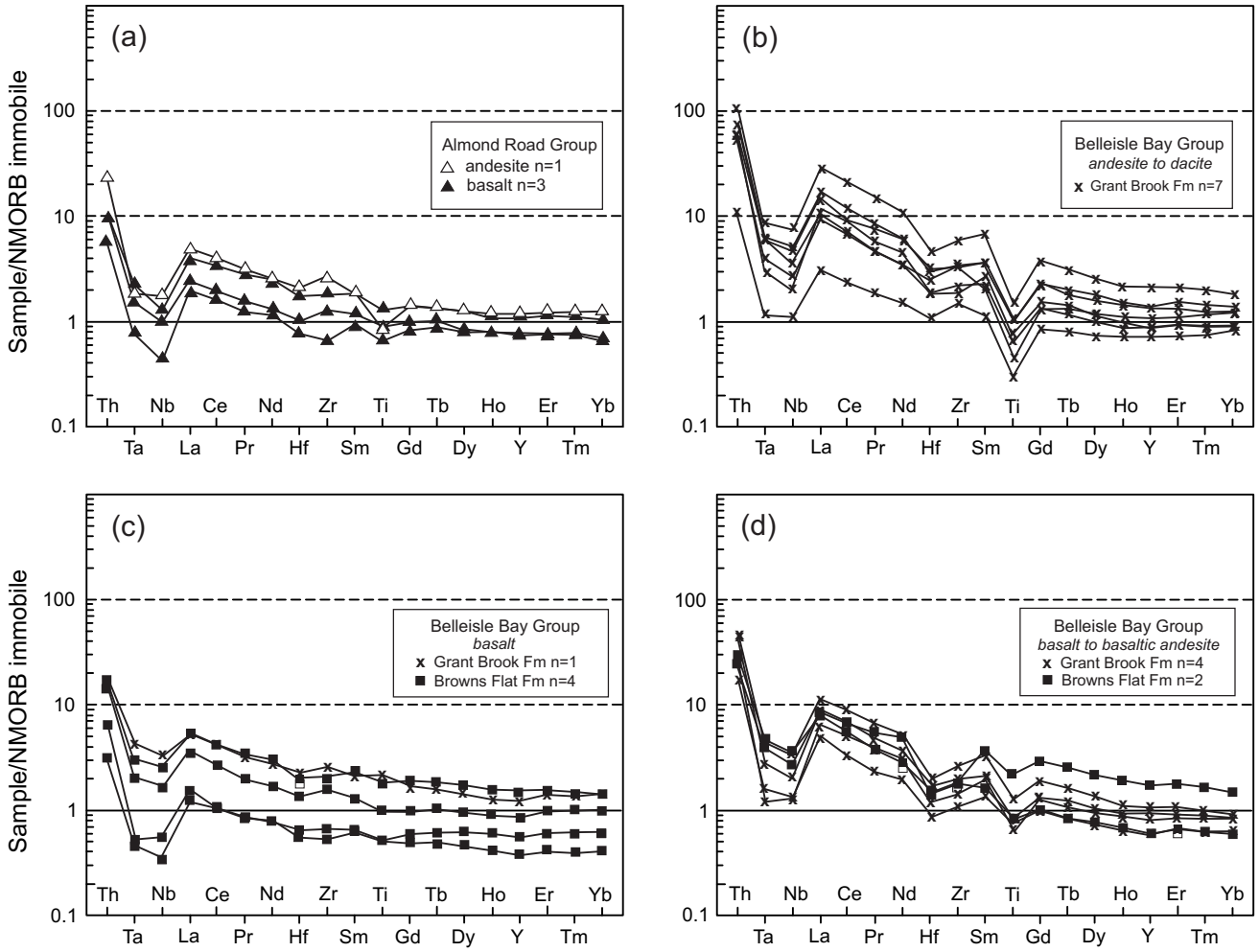

Figure 11. N-MORB-normalized spider diagrams after Sun and McDonough (1989) in Pearce (2014) showing mafic to intermediate volcanic rocks of the Almond Road and Belleisle Bay groups: (a) Almond Road Group andesite and basalt; (b) Grant Brook Formation andesite to dacite; and (c, d) Grant Brook and Browns Flat formations basalt to basaltic andesite.

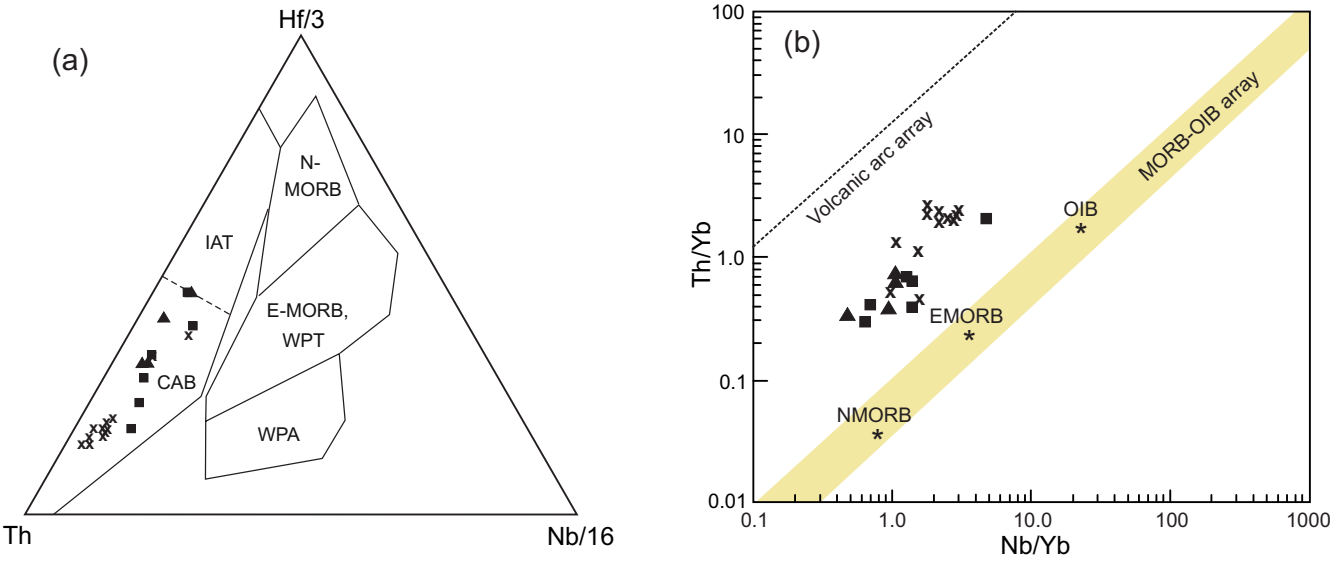

Figure 12. Tectonic discrimination diagrams comparing the Almond Road and Belleisle Bay groups: (a) ternary Th-Hf-Nb diagram with fields defined by Wood (1980) and (b) bivariate Th/Yb vs Nb/Y diagram after Pearce (2008). Abbreviations: CAB – calc-alkaline basalt; E-MORB – enriched mid-ocean ridge basalt; N-MORB – normal mid-ocean ridge basalt; IAT – island arc tholeiite; WPA – within-plate alkalic basalt; WPT – within-plate tholeiitic basalt. Symbols same as in Figure 10.

Previously published chemical data for the Belleisle Bay Group to the southwest in the Long Reach area (Johnson and Barr 2004) are compared to the results of this study. The latest Neoproterozoic to earliest Cambrian volcanic succession in the Long Reach area were divided into the Browns Flat and Beulah Camp formations, which were later assigned to the Belleisle Bay Group by Johnson *et al.* (2009). The Beulah Camp Formation is lithologically similar to the Grant Brook Formation and this correlation is corroborated by the chemical data. Basalts from the Beulah Camp Formation, like those in the Grant Brook were also chemically similar to those in the Browns Flat Formation (Johnson and Barr 2004). Major and trace element signatures in the former indicate that it also was likely erupted in a continental margin subduction zone (Johnson and Barr 2004). The Browns Flat Formation basalts in that area showed two different geochemical trends, one indicative of a within-plate setting and the other exhibiting characteristics of highly unevolved basalts suggesting a complex tectonic history.

DISCUSSION AND CORRELATION

Early Cambrian quartz-rich clastic sedimentary successions that overlie latest Ediacaran to earliest Cambrian volcanic and volcaniclastic to arkosic sedimentary rocks of the Belleisle Bay Group occur in all three structural panels within the NRB (Fyffe *et al.* 2011; fig. 4). These quartz-rich successions include the Matthews Lake Formation of the Ellsworth Group, the Snider Mountain Formation of the Almond Road Group, and the Glen Falls Formation of the Saint John Group. The age of the Glen Falls Formation is bracketed by a ca. 530 Ma ash bed from near the base of the underlying Ratcliffe Brook Formation and a ca. 510 Ma ash bed in the overlying Hanford Brook Formation (Landing *et al.* 1998; Landing and Westrop 1998; Isachasen *et al.* 1994; Palacios *et al.* 2011, 2017). A similar age is indicated for the Matthews Lake Formation as the overlying Mosquito Lake Road Formation is ca. 514 Ma (McLeod *et al.* 2003) and the youngest detrital zircon in the Matthews Lake Formation is ca. 540 Ma, (Fyffe *et al.* 2009). Although beyond the scope of this paper it is interesting to note the Glen Falls Formation quartzite in the Caledonia Terrane near Saint John shows a nearly unimodal detrital zircon population at ca. 540 Ma (Barr *et al.* 2012), essentially identical to the population distribution of zircon in the Matthews Lake Formation in the NRB, suggesting a similar source in the Early Cambrian. The age of the Almond Road Group is now bracketed between the Early Cambrian (late Terreneuvian) and Early Ordovician (Tremadocian) indicating that it is possible that all three quartzite sequences in the NRB are Stages 2-3 of the Cambrian (using the time scale of Cohen *et al.* 2013).

The textural maturity and bedforms that characterize the Glen Falls Formation indicate that it was deposited in a near-shore, high energy marine environment (Tanoli and Pickerill 1987; Landing and Westrop 1998). Although detailed sedimentological analysis was not undertaken on the Snider Mountain or Matthews Lake formations preliminary observations suggest a somewhat more distal depositional environment for these rocks. The most obvious is the lack of large-scale trough cross-bedding or other indications of wave action or fluvial processes that would be present in a shallow marine setting and the Snider Mountain Formation on Jones Brook contains no conglomerate at all. Although primary sedimentary features are rarely preserved in the more strongly deformed Matthews Lake Formation, some of the conglomerates have a mud-rich matrix and lithologically varied clasts that may have been deposited as debris flows. The Matthews Lake Formation as a whole tends to be a thicker, somewhat finer grained, quartzose sandstone sequence with local conglomerate debris flows that pass upwards into Mosquito Lake Formation containing sandstone with iron-rich siltstone lenses suggesting deposition in relatively deeper water. This led Fyffe *et al.* (2009, 2011) to suggest that the Almond Road and Matthews Lake may be more outboard facies of the tidally-influenced quartzite of the Glen Falls Formation, therefore would represent outer and inner platform sequences, respectively, deposited on NRB basement during the latter part of the Early Cambrian.

The arc-like chemistry of the Belleisle Bay Group is similar to the chemistry of mafic volcanic rocks in the upper Almond Road Group and the younger Late Cambrian to Early Ordovician Annidale Group, which occurs in the adjacent lithotectonic belt. The Annidale Group preserves the remains of the Penobscot back arc basin and a record of the Early Ordovician Penobscot orogeny (Johnson *et al.* 2009; 2012), one of the oldest orogenic events within the Appalachian orogen (Zagorevski et al 2007; van Staal and Barr 2012). In New Brunswick, the Penobscot back arc basin is interpreted to have developed along a continental margin represented by the Proterozoic rocks of the NRB and Brookville belt (Johnson *et al.* 2009, 2012; Fyffe *et al.* 2011). The Ediacaran rocks in these belts are interpreted to represent ensialic arc magmatism along the margin of Amazonia before it separated from Gondwana and became the Ganderian microcontinent (e.g., van Staal *et al.* 2012 and references therein). The arc signature of the ca. 540 Ma volcanic rocks in the Belleisle Bay Group supports the idea that the NRB was part of this continental margin in the Late Neoproterozoic and earliest Cambrian. The upwards transition from volcaniclastic sandstone and redbeds in the upper part of the Belleisle Bay Group to the widespread occurrence of quartz-rich sedimentary rocks by late Terreneuvian (530–520 Ma) suggest a rift-to-drift transition, possibly signalling the breakup of Gondwana. In other areas of Ganderia arc magmatism was shut-off at around 540 Ma due to ridge-trench collision that transformed the Gander margin into a strike-slip regime (e.g., Rogers *et al.* 2006). Exhumation of older rocks within the arc during such a collision could explain the prominence of ca. 575 Ma detrital zircon in the Almond Road Group. Around 515 Ma the NRB underwent

renewed arc volcanism as represented by rocks in the upper part of the Almond Road Group and the Mosquito Lake Road Formation (Johnson and McLeod 1996). This magmatism may be related to the development of the Penobscot arc and the formation of the Annidale back-arc basin by the Late Cambrian (ca. 495 Ma) (Johnson *et al.* 2012).

Rocks spanning the time period between the ca. 515 Ma Mosquito Lake Road Formation and ca. 495 Ma Annidale Group are not present in the NRB but they do occur in Maine. The chemical and isotopic data for the ca. 509–502 Ma Ellsworth Schist and overlying Castine Volcanics (Stewart 1998) in Maine show they are not arc-related, but that they likely developed within a proto- oceanic rift, such as in the Gulf of California (Schulz *et al.* 2008). Fyffe *et al.* (2009) considered the lithological characteristics of the Ellsworth volcanic sequence in coastal Maine to be similar to the Matthews Lake and Mosquito Lake Road formations in the NRB but the sequences are not temporally equivalent, therefore it remains unclear clear if this accounts for the contrast in tectonic environment or if it is due to along strike differences in an extremely complex long-lived convergent margin such as the Early Paleozoic Gander margin.

ACKNOWLEDGMENTS

The authors would like to extend their appreciation to Sherri Furey and Amanda Langille at the U–Pb laboratory at Memorial University Newfoundland and laboratory staff at Texas A & M University. We thank Sandra Barr and Chris White for initiating the detrital zircon project and facilitat-ing the U–Pb dating at Texas A & M and Chris White for providing the Concordia diagram for the Snider Mountain Formation. Journal reviewers Les Fyffe and Doug Reusch made many thoughtful comments that significantly im-proved the manuscript. We also wish to acknowledge Mal-colm McLeod who conducted field mapping in this area and made many contributions to our understanding of the geology. Geochemical data diagrams were produced using Geochemical Data Toolkit (GCDKit).

REFERENCES

Barr, S.M. and White, C.E. 1996a. Tectonic setting of Avalonian volcanic and plutonic rocks in the Caledonian Highlands, southern New Brunswick, Canada. Canadian Journal of Earth Sciences, 33, pp. 156–168. https://doi.org/10.1139/e96-015

Barr, S.M. and White, C.E. 1996b. Contrasts in late Precambrian–early Paleozoic tectonothermal history between Avalon Composite Terrane (*sensu stricto*) and other peri-Gondwanan terranes in southern New Brunswick and Cape Breton Island, Canada. *In* Avalonian and related peri-Gondwanan terranes of the Circum- North Atlantic. *Edited by* R.D. Nance and M.D. Thompson. Geological Society of America, Special Paper 304, pp. 95–108. https://doi.org/10.1130/0-8137-2304-3.95

Barr, S.M., White, C.E., and Miller, B.V. 2002. The Kingston Terrane, southern New Brunswick, Canada: evidence for an Early Silurian volcanic arc. Geological Society of America Bulletin, 114, pp. 964–982.https://doi.org/10.1130/0016-7606(2002)114<0964:TKTSNB>2.0.CO;2

Barr, S.M., Hamilton, M.A., Samson, S.D., Satkoski, A.M., and White, C.E. 2012. Provenance variations in northern Appalachian Avalonia based on detrital zircon age patterns in Ediacaran and Cambrian sedimentary rocks, New Brunswick and Nova Scotia, Canada. Canadian Journal of Earth Sciences, 49, pp. 533–546. https://doi.org/10.1139/e11-070

Barr, S.M., White, C.E., Davis, D.W., McClelland, W.C., and van Staal, C.R. 2014a. Infrastructure and provenance of Ganderia: evidence from detrital zircon ages in the Brookville terrane, southern New Brunswick, Canada. Precambrian Research, 246, pp. 358–370. https://doi.org/10.1016/j.precamres.2014.03.022

Barr, S.M., Johnson, S.C., and White, C.E. 2014b. The ongoing Saint John geology enigma: Avalonia versus Ganderia in southern New Brunswick. Geological Association of Canada-Mineralogical Association of Canada, Field Trip Guidebook B6, 52 p.

Barr, S.M., Miller, B.V., White, C.E., Johnson, S.C., and Fyffe, L.R. 2014c. Age and provenance of detrital zircon in Precambrian–Lower Paleozoic sedimentary units in southern New Brunswick: preliminary results. *In* Abstracts 2014: Exploration, Mining and Petroleum New Brunswick. *Edited by* E.A. Keith. New Brunswick Department of Energy and Mines, Geoscience Report 2014–5, p. 3.

Barrett, T.J. and MacLean, W.H. 1994. Chemostratigraphy and hydrothermal alteration in exploration for VHMS deposits in greenstones and younger volcanic rocks. *In* Alteration and alteration processes associated with ore-forming systems. *Edited by* D.R. Lentz. Geological Association of Canada. Short Course Notes, v.11, pp. 433–467.

Barrett, T.J. and MacLean, W.H. 1999. Volcanic sequences, lithogeochemistry, and hydrothermal alteration in some bimodal volcanic-associated massive sulphide systems. *In* Volcanic-associated massive sulphide deposits: processes and examples in modern and ancient settings. *Edited by* C.T. Barrie and M.D. Hannington. Reviews in Economic Geology, 8, pp. 101–131.

Black, L.P., Kamo, S.L., Allen, C.M., Davis, D.W., Aleinikoff, J.N., Valley, J.W., Mundil, R., Campbell, I.H., Korsch, R.J., Williams, I.S., and Foudoulis, C. 2004. Improved $^{206}Pb/^{238}U$ microprobe geochronology by the monitoring of a trace-element-related matrix effect; SHRIMP, ID-TIMS, ELA-ICP-MS and oxygen isotope documentation for a series of zircon standards. Chemical Geology, 205, pp. 115–140. https://doi.org/10.1016/j.chemgeo.2004.01.003

Cohen, K.M., Finney, S.C., Gibbard, P.L., and Fan, J.-X. (2013; updated) The ICS International Chronostratigraphic Chart. Episodes, 36, pp. 199–204.

Fyffe, L.R. and Fricker, A. 1987. Tectonostratigraphic terrane analysis of New Brunswick. Maritime Sediments and Atlantic Geology, 23, pp. 113–123. https://doi. org/10.4138/1626

Fyffe, L.R., Pickerill, R.K., and Stringer, P. 1999. Stratigraphy, sedimentology and structure of the Oak Bay and Waweig formations, Mascarene basins: implications for the Paleotectonic evolution of southwestern New Brunswick. Atlantic Geology, 35, pp. 59–84. https://doi.org/10.4138/2024

Fyffe, L.R., Barr, S.M., Johnson, S.C., McLeod, M.J., McNicoll, V.J., Valverde-Vaquero, P., van Staal, C.R., and White, C.R. 2009. Detrital zircon ages from Neoproterozoic and Early Paleozoic conglomerate and sandstone units of New Brunswick and coastal Maine: implications for the tectonic evolution of Ganderia. Atlantic Geology, 45, pp. 110–144. https://doi. org/10.4138/atlgeol.2009.006

Fyffe, L.R., Johnson, S.C., and van Staal, C.R. 2011. A review of Proterozoic to Early Paleozoic lithotectonic terranes in the northeastern Appalachian orogen of New Brunswick, Canada, and their tectonic evolution during Penobscot, Taconic, Salinic, and Acadian orogensis. Atlantic Geology, 47, pp. 211–248. https://doi.org/10.4138/atlgeol.2011.010

Hibbard, J.P., van Staal, C.R., Rankin, D.W., and Williams, H. 2006. Lithotectonic map of the Appalachian orogen, Canada — United States of America: Geological Survey of Canada, Map 02096A, 2 sheets, scale 1:1 500 000.

Hiess, J., Condon, D.J., McLean, N., and Noble, S.R. 2012. $^{238}U/^{235}U$ systematics in terrestrial uranium-bearing minerals. Science, 335, pp. 1610–1614. https://doi.org/10.1126/science.1215507

Isachsen, C. E., Bowring, S. A., Landing E., and Samson, S. D., 1994. New constraints on the division of Cambrian time. Geology, 22, pp. 496–498. https://doi.org/10.1130/0091-7613(1994)022<0496:NCOTDO>2.3.CO;2

Jaffey, A.H., Flynn, K.F., Glendenin, L.E., Bentley, W.C., and Essling, A.M. 1971. Precision measurement of half-lives and specific activities of ^{235}U and ^{238}U. Physical Review C: Nuclear Physics, 4, pp. 1889–1906. https://doi.org/10.1103/PhysRevC.4.1889

Johnson, S.C. 2001. Contrasting geology in the Pocologan River and Long Reach areas: implications for the New River belt and correlations in southern New Bruns-wick and Maine. Atlantic Geology, 37, pp. 61–79. https://doi.org/10.4138/1972

Johnson, S.C. and McLeod, M.J. 1996. The New River Belt: a unique segment along the western margin of the Avalon composite terrane, southern New Brunswick, Canada. *In* Avalonian and related peri-Gondwanan terranes of the Circum-North Atlantic. *Edited by* R.D. Nance and M.D. Thompson. Geological Society of America, Special Paper 304, pp. 149–164. https://doi.org/10.1130/0-8137-2304-3.149

Johnson, S.C. and Barr, S.M. 2004. New chemical data from from Neoproterozoic–Cambrian igneous rocks in the Long Reach area, southern New Brunswick. *In* Geological investigations in New Brunswick for 2003. *Edited by* G.L. Martin. New Brunswick Department of Natural Resources; Minerals, Policy, and Planning Division, Mineral Resource Report 2004–4, pp. 75–94.

Johnson, S.C., McLeod, M.J., Fyffe, L.R., and Dunning, G.R. 2009. Stratigraphy, geochemistry, and geochronology of the Annidale and New River belts, and the development of the Penobscot arc in southern New Brunswick. *In* Geological investigations in New Brunswick for 2008. *Edited by* G.L. Martin. New Brunswick Department of Natural Resources; Minerals, Policy, and Planning Division. Mineral Resource Report 2009–2, pp. 141–218.

Johnson, S.C., Fyffe, L.R., McLeod, M.J., and Dunning, G.R. 2012. U–Pb ages, and tectonomagmatic history of the Cambro–Ordovician Annidale group: a remnant of the Penobscot arc system in southern New Brunswick. Canadian Journal of Earth Sciences, 49, pp. 166–188.

Landing, E. and Westrop, S. R. 1998. Cambrian faunal sequences and depositional history of Avalonian Newfoundland and New Brunswick: field workshop. *In* Avalon 1997 – The Cambrian Standard. *Edited by* E. Landing and S.R. Westrop. New York State Museum Bulletin, 492 p.

Landing, E., Bowring, S. A., Davidek, K. L., Westrop, S. R., Geyer, G., and Heldmaier, W. 1998. Duration of the Early Cambrian: U–Pb ages of volcanic ashes from Avalon and Gondwana. Canadian Journal of Earth Sciences, 35, pp. 329–338. https://doi.org/10.1139/e97-107

Mattinson, J.M. 2005. Zircon U–Pb chemical-abrasion (CA-TIMS) method: combined annealing and multi-step dissolution analysis for improved precision and accuracy of zircon ages. Chemical Geology, 220, pp. 47–66. https://doi.org/10.1016/j.chemgeo.2005.03.011

McCutcheon, S.R. and Ruitenberg, A.A. 1987. Geology and mineral deposits, Annidale–Nerepis area, New Brunswick. New Brunswick Department of Natural Resources and Energy; Mineral Resources Division, Memoir 2, 141 p.

McLeod, M.J., Johnson, S.C., and Krogh, T.E. 2003. Archived U–Pb (zircon) dates from southern New Brunswick. Atlantic Geology, 39, pp. 209–225. https://doi.org/10.4138/1182

Paces, J.B. and Miller, J.D. 1993. Precise U–Pb ages of of Duluth Complex and related mafic intrusions, northeastern Minnesota: geochronological in-sights into physical, petrogenetic, paleomagnetic and tectonomagmatic processes associated with the 1.1 Ga mid-

-continent rift system. Journal of Geo-physical Research, 98, pp.13997–14013. https://doi. org/10.1029/93JB01159

Palacios, T., Jensen, S., Barr, S.M., White, C.E., and Miller, R.F. 2011. New biostratigraphical constraints on the lower Cambrian Ratcliffe Brook Formation, southern New Brunswick, Canada, from organic-walled microfossils. Stratigraphy, 8, pp.45–60.

Palacios, T., Jensen, S., Barr, S.M., White, C.E., and Miller, R.F. 2017. Acritarchs from the Hanford Brook Formation, New Brunswick, Canada: new biochronological constraints on the *Protolenus elegans* Zone and the Cambrian Series 2–3 transition. Geological Magazine, 154, pp. 571–590. https://doi.org/10.1017/S0016756816000224

Paton, C., Woodhead, J., Hellstrom, J., Hergt, J.M., Greig, A. and Maas, R. 2010. Improved laser ablation U–Pb zircon geochronology through robust downhole fractionation correction. Geochemistry, Geophysics, Geosystems, 11, Q0AA06, 36 pp. https://doi. org/10.1029/2009GC002618

Paton, C., Hellstrom, J., Paul, B., Woodhead, J. and Hergt, J.M. 2011. Iolite: freeware for the visualisation and processing of mass spectrometric data. Journal of Analytical Atomic Spectrometry, 26, pp. 2508–2518. https://doi.org/10.1039/c1ja10172b

Pearce, J.A. 1996. A user's guide to basalt discrimination diagrams. *In* Trace element geochemistry of volcanic rocks: applications for massive sulphide exploration. *Edited by* D.A. Wyman. Geological Association of Canada/Mineralogical Association of Canada, short course notes, 12, pp. 79–113.

Pearce, J.A. 2014. Immobile element fingerprinting of ophiolites. Elements, 10, pp. 101–108. https://doi.org/10.2113/gselements.10.2.101

Pearce, J.A. and Peate,D.W. 1995. Tectonic implications of the composition of volcanic arc magmas. Annual Review of Earth and Planetary Science, 23, pp. 251–285. https://doi.org/10.1146/annurev.ea.23.050195.001343

Pearce, J.A. 2008. Geochemical fingerprinting of oceanic basalts with applications to ophiolite classification and the search for Archean oceanic crust. Lithos, 100, pp. 14–48. https://doi.org/10.1016/j.lithos.2007.06.016

Rogers, N., van Staal, C.R., McNicoll, V., Pollock, S.J., Zagorevski, A., and Whalen, J. 2006. Neoproterozoic and Cambrian arc magmatism along the eastern margin of the Victoria Lake Supergroup: a remnant of Ganderian basement in central Newfoundland? Precambrian Research, 147, pp. 320–341. https://doi.org/10.1016/j.precamres.2006.01.025

Ross, P.S. and Bédard, J.H. 2009. Magmatic affinity of modern and ancient subalkaline volcanic rocks determined from trace-element discriminant diagrams. Canadian Journal of Earth Sciences, 46, pp. 823–839. https://doi.org/10.1139/E09-054

Sánchez-García, T., Quesada, C., Bellido, F., Dunning, G.R., G.R., and González del Tánago, J. 2008. Two-step magma flooding of the upper crust during rifting: the early Paleozoic of the Ossa Morena Zone (SW Iberia). Tectonophysics, 461, pp. 72–90. https://doi. org/10.1016/j.tecto.2008.03.006

Schulz, K.J., Stewart, D.B., Tucker, R.D., Pollock, J.C., and Ayuso, R.A. 2008. The Ellsworth terrane, coastal Maine. Geochronology, geochemistry, and Nd-Pd isotopic compositions - Implications for the rifting of Ganderia. Geological Society of America Bulletin, 120, pp. 1134–1158. https://doi.org/10.1130/B26336.1

Stacey, J.S. and Kramers, J.D. 1975. Approximation of terrestrial lead isotope evolution by a two-stage model. Earth and Planetary Science Letters, 26, pp. 207–221. https://doi.org/10.1016/0012-821X(75) 90088-6.

Stewart, D.B. 1998. Geology of Northern Penobscot Bay, Maine: U.S. Geological Survey Miscellaneous Investigations Series Map I-2551, 2 sheets, scale 1:62 500.

Sun, S.S. and McDonough, W.F. 1989. Chemical and isotopic systematics of oceanic basalts: implications for mantle composition and processes. *In* Magmatism in the ocean basins. *Edited by* A.D. Saunders and M.J. Norry. Geological Society of London Special Publication 42, pp. 313–345. https://doi.org/10.1144/GSL.SP.1989.042.01.19

Tanoli, S.K. and Pickerill, R.K. 1987. The Glen Falls Formation – an example of a barrier island retreated by shoreface erosion. Geological Bulletin, University of Peshawar, 20, pp. 1–21.

Tanoli, S.K. and Pickerill, R.K. 1988. Lithostratigraphy of the Cambrian-Lower Ordovician Saint John Group, southern New Brunswick. Canadian Journal of Earth Sciences, 2, pp. 669–690. https://doi.org/10.1139/e88-064

Van Staal, C.R. and Barr, S.M. 2012. Lithospheric architecture and tectonic evolution of the Canadian Appalachians. *In* Tectonic styles in Canada revisited: the Lithoprobe perspective. *Edited by* J. A. Percival, F.A. Cook, and R. M. Clowes. Geological Association of Canada, Special Paper 49, p. 41–95.

Van Staal, C.R., Wilson, R.A., Rogers, N., Fyffe, L.R., Langton, J.P., McCutcheon, S.R., McNicoll, V., and Ravenhurst, C.E. 2003. Geology and tectonic history of the Bathurst Supergroup, Bathurst Mining Camp and its relationships to coeval rocks in southwestern New Brunswick and adjacent Maine-a synthesis. *In* Massive sulfide deposits of the Bathurst Mining Camp, New Brunswick and northern Maine. *Edited by* W.D. Goodfellow, S.R. McCutcheon, and J.M. Peter. Economic Geology Monograph 11, p. 37–60.

Van Staal, C.R., Barr, S.M., and Murphy, B.J. 2012. Provenance and tectonic evolution of Ganderia: constraints on the evolution of the Iapetus and Rheic oceans. Geology, 40, pp. 987–990. https://doi.org/10.1130/G33302.1

Wiedenbeck, M., Alle, P., Corfu, F., Griffin, W.L., Meier, M., Oberli, F., von Quadt, A., Roddick, J.C., and Spiegel, W. 1995. Three natural zircon standards for U–Th–Pb, Lu–Hf, trace element and REE analy-ses. Geostandards Newsletter 19, 1–23. https://doi.org/10.1111/j.1751-908X.1995.tb00147.x

Wilson, R.A. 2003. Geochemistry and petrogenesis of Ordovician arc-related mafic volcanic rocks in the Popelogan Inlier, northern New Brunswick. Canadian Journal of Earth Sciences, 40, pp. 1171–1189. https://doi.org/10.1139/e03-034

Winchester, J.A. and Floyd, P.A. 1977. Geochemical discrimination of different magma series and their differentiation products using immobile elements. Chemical Geology, 20, pp. 325–343. https://doi.org/10. 1016/0009-2541(77)90057-2

Wood, D.A. 1980. The application of a Th–Hf–Ta diagram to problems of tectonomagmatic classification and to establishing the nature of crustal contamination of basaltic lavas of the British Tertiary volcanic province. Earth and Planetary Science Letters, 50, pp. 11–30. https://doi.org/10.1016/0012-821X(80)90116-8

Zagorevski, A., van Staal, C.R., Rogers, N., McNicoll, V.J., and Pollock, J. 2010. Middle Cambrian to Ordovician arc-backarc development on the leading edge of Ganderia, Newfoundland Appalachians *In* From Rodinia to Pangea: the lithotectonic record of the Appalachian Region. *Edited by* R.P. Tollo, M.J. Bartholomew, J.P Hibbard, and P.M. Karabinos. Geological Society of America, Memoir 206, pp. 367–396. https://doi.org/10.1130/2010.1206(16)

Zagorevski, A., van Staal, C.R., and McNicoll, V.J. 2007. Distinct Taconic, Salinic and Acadian deformation along the Iapetus suture zone, Newfoundland Appalachians. Canadian Journal of Earth Sciences, 44, pp. 1567–1585. https://doi.org/10.1139/e07-037

Editorial responsibility: David P. West, Jr.

Appendix A. U-Th-Pb detrital zircon isotope analyses for NB12-313.

Analysis Identifier (NB313)	Pb[1]	U[1] (ppm)	Th[1]	Isotope Ratios[2]												Ages (Ma)[3]									
				$^{206}Pb/^{204}Pb$	$^{208}Pb/^{206}Pb$	$\pm 2\sigma^2$	$^{208}Pb/^{232}Th$	$\pm 2\sigma^2$	$^{207}Pb/^{206}Pb$	$\pm 2\sigma^2$	$^{207}Pb/^{235}U$	$\pm 2\sigma^2$	$^{206}Pb/^{238}U$	$\pm 2\sigma^2$	Rho[3]	$^{208}Pb/^{232}Th$	$\pm 2\sigma^2$	$^{207}Pb/^{206}Pb$	$\pm 2\sigma^2$	$^{207}Pb/^{235}U$	$\pm 2\sigma^2$	$^{206}Pb/^{238}U$	$\pm 2\sigma^2$	% disc.[4]
a_01	224.5	247.7	253.0	19000	3.366	0.065	0.0935	0.004	0.1096	0.0012	4.887	0.084	0.3206	0.0029	0.82772	1807	78	1790	20	1799.4	14	1793	14	0.36
a_02	74.9	331.0	258.1	11900	3.63	0.078	0.0294	0.001	0.0597	0.0011	0.768	0.017	0.0927	0.0013	0.55915	586	28	585	39	578.3	9.8	571.2	7.4	1.23
a_03	27.3	199.0	104.8	9400	5.62	0.12	0.0267	0.001	0.0582	0.0011	0.698	0.015	0.0865	0.00088	0.47591	531.8	25	526	43	537	9.1	534.8	5.2	0.41
a_07	64.0	185.8	85.2	17000	6.91	0.14	0.0769	0.004	0.0976	0.0014	3.723	0.078	0.2742	0.0032	0.75536	1497	72	1574	28	1575	17	1562	16	0.83
a_09	94.2	484.0	351.0	14000	4.239	0.088	0.0271	0.001	0.0588	0.001	0.719	0.015	0.08836	0.00086	0.59279	540	25	551	33	549.5	8.4	545.8	5.1	0.67
a_10	89.5	445.0	347.0	19000	3.75	0.085	0.026	0.001	0.0603	0.0011	0.715	0.018	0.0851	0.0013	0.69431	519.2	24	614	39	547.3	11	526.6	7.5	3.78
a_11	192.0	560.0	189.0	160000	9.58	0.99	0.1017	0.005	0.1198	0.0021	5.92	0.16	0.3567	0.009	0.77707	1957	90	1951	31	1963	23	1965	43	-0.10
a_12	171.2	399.0	196.3	101000	6.42	0.16	0.09	0.004	0.1064	0.0014	4.601	0.11	0.3119	0.0056	0.83962	1741	79	1735	25	1748	20	1750	27	-0.11
a_13	57.7	424.0	172.4	29000	7.48	0.26	0.0353	0.002	0.0651	0.00083	1.017	0.019	0.1131	0.001	0.80048	701	33	771	26	713.2	9.8	690.9	5.9	3.13
a_14	20.6	141.0	74.8	7900	6.09	0.29	0.0292	0.002	0.0625	0.0015	0.791	0.02	0.09132	0.00099	0.32985	581	29	680	51	591.1	11	563.3	5.9	4.70
a_15	115.0	155.0	106.0	17600	5.3	0.24	0.1087	0.005	0.1236	0.0017	6.201	0.11	0.3624	0.0042	0.63189	2091	97	2004	25	2005	15	1996	19	0.45
a_16	247.0	757.0	665.0	77000	3.125	0.098	0.0368	0.002	0.0659	0.0013	1.084	0.036	0.1191	0.004	0.82562	731	36	797	42	745	17	725	23	2.68
a_17	79.7	414.0	114.6	78000	11.64	0.16	0.0716	0.003	0.0853	0.00092	2.857	0.049	0.2425	0.0023	0.82343	1397	62	1320	21	1369.8	13	1399	12	-2.13
a_18	58.1	309.0	203.9	24000	4.62	0.075	0.0293	0.001	0.0592	0.00087	0.7825	0.015	0.09546	0.00093	0.66029	584.4	27	568	31	586.5	8.3	587.7	5.5	-0.20
a_19	37.6	272.0	130.3	23000	5.66	0.19	0.029	0.002	0.0611	0.0014	0.767	0.023	0.0902	0.002	0.65111	577	32	634	51	577	13	557	12	3.47
a_21	113.7	412.0	393.0	45000	2.962	0.097	0.0296	0.001	0.0622	0.0011	0.812	0.021	0.0945	0.0017	0.73049	590	28	683	35	602.7	12	582	9.9	3.43
a_23	68.1	318.0	272.0	43000	3.581	0.064	0.0262	0.001	0.0581	0.0011	0.682	0.016	0.0851	0.001	0.59856	522.3	24	524	42	527.3	9.4	526.2	6.1	0.21
a_24	111.2	527.0	130.0	160000	12.54	0.43	0.0875	0.004	0.1026	0.0014	4.161	0.099	0.294	0.0057	0.81921	1696	77	1669	25	1664	20	1660	29	0.24
a_25	157.0	450.0	596.0	58000	2.58	0.1	0.0284	0.001	0.0601	0.00085	0.761	0.015	0.0919	0.0011	0.70253	564.9	26	601	31	574.4	8.7	566.4	6.5	1.39
a_26	61.9	259.0	198.1	38000	4.093	0.081	0.0328	0.002	0.0635	0.0012	0.929	0.022	0.1062	0.0011	0.63389	653	30	719	40	666.4	11	650.8	6.4	2.34
a_28	55.3	236.2	197.2	22000	3.72	0.15	0.029	0.001	0.0591	0.001	0.779	0.018	0.0957	0.0014	0.68238	578	27	562	38	584.1	10	589	8.2	-0.84
a_29	29.6	139.5	103.4	22300	4.04	0.1	0.0293	0.001	0.061	0.0012	0.797	0.019	0.0949	0.0011	0.57121	583	28	628	43	594.6	11	584.6	6.5	1.68
a_30	70.3	262.2	250.8	18000	3.138	0.087	0.0291	0.001	0.0636	0.0016	0.817	0.024	0.0932	0.0013	0.51814	580	28	718	54	605	13	574.2	7.5	5.09
b_31	218.0	960.0	297.0	142000	10.08	0.15	0.0757	0.003	0.0916	0.00092	3.335	0.054	0.2653	0.0025	0.81964	1475	64	1459	18	1488.6	13	1517	12	-1.91
b_32	169.0	732.0	654.0	33000	3.36	0.21	0.026	0.001	0.0667	0.0017	0.817	0.028	0.0894	0.0026	0.68764	518	26	823	54	606	16	552	15	8.91
b_33	58.5	285.0	214.0	11700	4.14	0.18	0.0278	0.001	0.0607	0.0012	0.738	0.018	0.089	0.0011	0.59183	553	26	618	42	560.7	11	549.3	6.8	2.03
b_34	29.5	140.0	117.4	6600	3.79	0.14	0.0263	0.001	0.0588	0.0012	0.694	0.016	0.0861	0.001	0.46668	525	25	544	45	534.4	9.6	532.6	6	0.34
b_36	127.8	325.0	150.8	27100	6.58	0.13	0.0874	0.004	0.1085	0.0015	4.475	0.093	0.2996	0.0038	0.76186	1694	75	1772	25	1725	17	1689	19	2.09

Appendix A. Continued.

Analysis Identifier (NB313)	Pb[1]	U[1] (ppm)	Th[1]	Isotope Ratios[2]												Ages (Ma)[3]										% disc.[4]
				$^{206}Pb/^{204}Pb$	$^{208}Pb/^{206}Pb$	± 2σ[2]	$^{208}Pb/^{232}Th$	± 2σ[2]	$^{207}Pb/^{206}Pb$	± 2σ[2]	$^{207}Pb/^{235}U$	± 2σ[2]	$^{206}Pb/^{238}U$	± 2σ[2]	Rho[3]	$^{208}Pb/^{232}Th$	± 2σ[2]	$^{207}Pb/^{206}Pb$	± 2σ[2]	$^{207}Pb/^{235}U$	± 2σ[2]	$^{206}Pb/^{238}U$	± 2σ[2]	
b_38	30.3	117.4	114.7	6400	3.24	0.067	0.0275	0.001	0.0579	0.0011	0.73	0.017	0.09162	0.00097	0.59515	548	26	517	43	555.5	10	565	5.7	-1.71
b_39	46.7	274.0	175.9	3900	4.62	0.14	0.0269	0.001	0.0594	0.0012	0.745	0.021	0.0909	0.002	0.70182	537	28	587	49	564	12	561	12	0.53
b_40	298.3	833.0	465.0	38000	6.28	0.22	0.0645	0.003	0.0998	0.0014	3.613	0.09	0.2636	0.0051	0.82794	1262	64	1618	26	1551	20	1508	26	2.77
b_41	45.6	417.0	174.2	12000	7.62	0.44	0.0281	0.002	0.0598	0.0011	0.73	0.022	0.0887	0.0016	0.82342	560	29	591	40	556	13	548	9.4	1.44
b_42	91.6	350.0	357.0	16000	3.35	0.14	0.0276	0.001	0.0592	0.001	0.736	0.016	0.09043	0.00079	0.69291	550	26	566	38	559.7	9.1	558	4.7	0.30
b_44	116.7	190.3	145.1	35000	4.281	0.073	0.0834	0.004	0.0984	0.0013	3.965	0.076	0.2938	0.0033	0.7409	1618	72	1590	25	1626	16	1660	16	-2.09
b_45	28.6	123.0	105.6	7300	3.62	0.16	0.0284	0.002	0.0606	0.0015	0.763	0.022	0.0909	0.0015	0.51596	566	29	617	55	574	13	561	8.6	2.26
b_46	38.0	191.0	131.0	14800	4.6	0.19	0.0302	0.002	0.0594	0.0009	0.768	0.017	0.0944	0.0015	0.72878	602	31	577	34	577.8	9.6	581.5	8.6	-0.64
b_47	98.6	403.2	365.6	11000	3.432	0.055	0.0281	0.001	0.0599	0.00081	0.755	0.015	0.0915	0.0011	0.74644	559	25	599	30	570.7	8.9	564	6.7	1.17
b_48	308.0	890.0	362.0	170000	7.91	0.12	0.0875	0.004	0.1031	0.0012	4.409	0.077	0.3107	0.0033	0.76106	1695	74	1678	22	1713.2	15	1744	16	-1.80
b_49	83.3	759.0	145.1	26000	15.66	0.64	0.06	0.003	0.0762	0.0011	1.988	0.048	0.1889	0.003	0.81696	1177	53	1096	28	1110	16	1119	18	-0.81
b_50	97.3	388.3	351.0	20000	3.62	0.14	0.0293	0.001	0.0607	0.0012	0.822	0.019	0.0984	0.0016	0.54257	583	28	624	41	609	11	605.1	9.5	0.64
b_52	41.9	168.1	169.9	13900	3.422	0.091	0.0264	0.001	0.0636	0.0016	0.77	0.02	0.0879	0.0012	0.32169	527	26	719	53	579	12	543.2	6.8	6.18
b_53	158.9	1257.0	537.0	59000	6.46	0.2	0.0296	0.002	0.0617	0.0011	0.803	0.022	0.0946	0.0021	0.76091	590	29	659	37	598	13	582	12	2.68
b_55	61.7	295.0	197.0	25000	4.587	0.082	0.0326	0.002	0.0612	0.00098	0.905	0.017	0.1072	0.0016	0.56867	648	30	637	34	654.2	9.2	656.1	9.3	-0.29
b_56	63.1	260.3	227.0	18000	3.56	0.096	0.0296	0.002	0.0603	0.0013	0.755	0.02	0.0909	0.0011	0.59798	590	29	609	45	570.8	12	560.6	6.5	1.79
b_57	23.9	87.0	83.9	6200	3.39	0.15	0.0304	0.002	0.0627	0.0023	0.824	0.03	0.0956	0.0014	0.18228	605	34	675	77	609	16	588.6	8.2	3.35
b_58	131.8	486.5	450.0	34000	3.142	0.063	0.0299	0.001	0.0596	0.0013	0.791	0.024	0.0966	0.0022	0.69717	596	28	580	46	591	13	594	13	-0.51
b_59	48.0	194.0	172.0	27000	3.209	0.098	0.029	0.001	0.0608	0.0016	0.745	0.023	0.0893	0.0012	0.5317	578	28	617	56	564	13	551.6	7.3	2.20
b_60	113.2	395.0	465.0	26000	2.83	0.14	0.0257	0.001	0.06	0.0011	0.6857	0.013	0.0832	0.00092	0.34725	511.9	23	592	37	529.8	8.1	515.1	5.5	2.77
c_61	58.9	271.5	217.0	17000	4.06	0.14	0.0286	0.001	0.0593	0.0009	0.766	0.015	0.09429	0.00098	0.64136	569	26	574	32	577.9	8.7	580.8	5.8	-0.50
c_62	82.9	578.0	306.0	58000	5.816	0.095	0.0285	0.001	0.0594	0.00068	0.7479	0.013	0.09132	0.00097	0.76873	567.6	26	577	25	566.7	7.8	563.3	5.7	0.60
c_63	74.9	434.6	281.0	14000	4.69	0.16	0.0277	0.001	0.059	0.0011	0.731	0.019	0.09	0.0014	0.70483	551.2	26	560	41	556.3	11	555.3	8.2	0.18
c_64	71.9	324.0	247.0	39000	3.88	0.13	0.03	0.001	0.0611	0.0012	0.794	0.018	0.0943	0.0011	0.49968	598	28	634	42	593.1	10	581	6.6	2.04
c_65	201.0	77.6	268.0	17000	1.045	0.098	0.0791	0.004	0.0958	0.0015	3.481	0.072	0.2658	0.0033	0.65577	1538	68	1537	30	1521	16	1519	17	0.13
c_66	95.7	295.0	339.0	20000	2.729	0.069	0.0297	0.001	0.0595	0.00091	0.78	0.018	0.0953	0.0014	0.75851	592	28	581	32	584.8	10	586.8	8	-0.34
c_67	156.0	492.0	568.0	32000	2.886	0.084	0.0288	0.001	0.0605	0.00072	0.7935	0.014	0.09504	0.00088	0.78109	573.6	26	623	26	592.8	8.1	585.2	5.2	1.28
c_68	93.7	321.0	346.0	40000	3.011	0.09	0.0284	0.001	0.0599	0.001	0.774	0.019	0.0936	0.0014	0.74547	566	27	590	37	581.2	11	576.5	8	0.81

Appendix A. Continued.

Analysis Identifier (NB313)	Pb[1]	U[1] (ppm)	Th[1]	Isotope Ratios[2]												Ages (Ma)[3]									
				$^{206}Pb/^{204}Pb$	$^{208}Pb/^{206}Pb$	$\pm 2\sigma^2$	$^{208}Pb/^{232}Th$	$\pm 2\sigma^2$	$^{207}Pb/^{206}Pb$	$\pm 2\sigma^2$	$^{207}Pb/^{235}U$	$\pm 2\sigma^2$	$^{206}Pb/^{238}U$	$\pm 2\sigma^2$	Rho[3]	$^{208}Pb/^{232}Th$	$\pm 2\sigma^2$	$^{207}Pb/^{206}Pb$	$\pm 2\sigma^2$	$^{207}Pb/^{235}U$	$\pm 2\sigma^2$	$^{206}Pb/^{238}U$	$\pm 2\sigma^2$	% disc.[4]
c_71	31.5	1016.0	22.8	93000	44.7	9.3	0.159	0.049	0.0711	0.0024	1.103	0.038	0.1128	0.0014	0.23566	3080	850	948	65	754	18	689.2	7.9	8.59
c_72	63.3	181.0	247.0	80000	2.608	0.085	0.0275	0.001	0.0627	0.00098	0.806	0.016	0.09379	0.00097	0.62544	548	26	690	33	599.6	9.2	577.8	5.7	3.64
c_73	75.1	313.0	262.0	46000	3.47	0.1	0.0297	0.002	0.0668	0.0017	0.856	0.027	0.0939	0.0017	0.59103	591	29	820	53	627	15	579	10	7.66
c_75	138.0	401.0	511.0	42000	2.71	0.2	0.0286	0.002	0.0635	0.0014	0.827	0.021	0.095	0.0022	0.59095	570	29	718	45	611.1	12	585	13	4.27
c_80	261.9	755.0	783.0	500000	2.82	0.059	0.0363	0.002	0.0594	0.0013	0.849	0.024	0.1039	0.0023	0.64733	721	41	578	47	624	13	637	14	-2.08
c_81	57.5	204.7	213.4	68000	3.015	0.082	0.029	0.002	0.0641	0.0015	0.796	0.026	0.0902	0.0018	0.70381	577	30	736	49	593	14	557	11	6.07
c_82	56.7	287.4	220.8	45000	4.129	0.094	0.0266	0.001	0.0611	0.0013	0.761	0.021	0.0905	0.0011	0.68057	530	26	634	45	574	12	558.6	6.3	2.68
c_84	62.6	148.0	82.7	210000	5.99	0.19	0.0807	0.004	0.1033	0.0018	3.787	0.075	0.267	0.0029	0.48014	1568	73	1680	31	1589	16	1525	15	4.03
c_86	98.7	380.0	92.7	250000	12.6	0.28	0.1118	0.005	0.13	0.0013	6.48	0.11	0.363	0.0029	0.92882	2142	93	2095	17	2042.4	14	1998	15	2.17
c_87	27.8	132.0	91.0	28000	4.93	0.15	0.032	0.002	0.0643	0.0014	0.937	0.02	0.1065	0.0013	0.25051	637	30	737	43	670.6	10	652	7.3	2.77
c_89	1063.0	2374.0	3600.0	298000	1.969	0.068	0.0301	0.001	0.0675	0.0015	0.922	0.024	0.1002	0.002	0.56023	599	28	847	45	663	13	615	12	7.24
d_100	79.8	264.1	315.5	48000	2.906	0.042	0.0274	0.001	0.0585	0.0012	0.722	0.017	0.08922	0.00099	0.49135	545.3	25	541	47	551.7	9.8	550.9	5.8	0.15
d_101	21.3	83.4	77.6	5300	3.49	0.11	0.029	0.002	0.06	0.0019	0.775	0.025	0.094	0.0011	0.23146	578	29	569	68	581	14	578.9	6.4	0.36
d_102	65.8	233.0	266.0	90000	2.99	0.11	0.0261	0.001	0.0597	0.0011	0.695	0.015	0.0849	0.001	0.52132	520	25	580	40	535.2	9.1	525.1	6	1.89
d_104	66.3	207.6	252.4	18000	2.666	0.051	0.0278	0.001	0.0598	0.0011	0.759	0.018	0.0918	0.0012	0.63698	554.7	25	598	43	572.8	11	565.9	7.1	1.20
d_106	303.0	643.0	352.0	102000	6.66	0.28	0.0918	0.004	0.1096	0.0011	5.006	0.087	0.3327	0.0031	0.88958	1775	79	1790	18	1819.3	15	1851	15	-1.74
d_107	271.0	602.0	860.0	20000	2.355	0.075	0.034	0.002	0.0689	0.0014	1.093	0.034	0.1153	0.0019	0.806	676	36	888	43	749	16	703	11	6.14
d_108	93.8	402.0	398.0	80000	3.482	0.099	0.0254	0.001	0.059	0.00079	0.693	0.014	0.0853	0.0011	0.75871	505.9	24	567	28	534.4	8.6	527.5	6.2	1.29
d_109	82.2	474.0	287.6	16000	5.16	0.11	0.0299	0.002	0.0626	0.0015	0.86	0.028	0.1008	0.0022	0.67705	595	34	684	49	629	15	619	13	1.59
d_110	88.2	218.6	148.5	10000	4.799	0.086	0.0626	0.003	0.0825	0.0015	2.449	0.062	0.2158	0.0032	0.70621	1226	61	1251	35	1256	18	1260	17	-0.32
d_111	36.1	115.3	140.6	5500	2.736	0.068	0.027	0.001	0.0611	0.0016	0.792	0.022	0.0944	0.0014	0.37117	538	28	631	54	591	13	581.5	8.1	1.61
d_112	130.6	262.4	191.4	29000	4.86	0.34	0.0713	0.004	0.0935	0.0013	3.313	0.087	0.2583	0.0056	0.84865	1391	67	1495	26	1486	19	1480	29	0.40
d_113	482.0	232.0	510.0	50000	1.755	0.051	0.1008	0.005	0.1249	0.0012	6.448	0.11	0.3766	0.0036	0.88942	1942	84	2025	18	2037.8	15	2060	17	-1.09
d_116	38.8	147.2	60.3	11000	8.7	0.23	0.068	0.003	0.0888	0.0012	2.874	0.066	0.2335	0.003	0.86397	1330	65	1394	27	1373	17	1352	16	1.53
d_117	185.8	736.0	220.0	34400	11.14	0.32	0.0873	0.005	0.1183	0.0023	5.13	0.12	0.3162	0.0062	0.60355	1691	98	1927	33	1840	20	1770	30	3.80
d_118	185.0	748.0	768.0	16000	3.22	0.11	0.0253	0.001	0.0621	0.0012	0.733	0.02	0.0857	0.0012	0.74222	505	24	671	41	557.8	11	530	6.9	4.98
d_119	56.0	57.3	109.2	7200	1.757	0.051	0.054	0.003	0.0782	0.002	2.011	0.056	0.1878	0.0034	0.44541	1063	52	1137	52	1117	19	1109	18	0.72
d_91	70.2	283.2	269.0	50000	3.2	0.13	0.027	0.001	0.0623	0.0019	0.752	0.022	0.0876	0.0018	0.28944	539	28	670	65	569	13	541	10	4.92

Appendix A. Continued.

Analysis Identifier (NB313)	Pb[1]	U[1] (ppm)	Th[1]	Isotope Ratios[2]												Ages (Ma)[3]										% disc.[4]
				$^{206}Pb/^{204}Pb$	$^{208}Pb/^{206}Pb$	± 2σ[2]	$^{208}Pb/^{232}Th$	± 2σ[2]	$^{207}Pb/^{206}Pb$	± 2σ[2]	$^{207}Pb/^{235}U$	± 2σ[2]	$^{206}Pb/^{238}U$	± 2σ[2]	Rho[3]	$^{208}Pb/^{232}Th$	± 2σ[2]	$^{207}Pb/^{206}Pb$	± 2σ[2]	$^{207}Pb/^{235}U$	± 2σ[2]	$^{206}Pb/^{238}U$	± 2σ[2]	
d_94	174.0	676.0	588.0	117000	3.38	0.1	0.03	0.002	0.0671	0.0014	0.917	0.025	0.0989	0.0021	0.6554	598	34	837	45	660	13	608	13	7.88
d_95	118.0	664.0	413.0	89000	5.1	0.24	0.0314	0.002	0.0631	0.0013	0.804	0.02	0.0922	0.0012	0.56174	625	30	705	43	598.5	11	568.6	7.3	5.00
d_96	77.0	257.0	268.0	100000	3.26	0.12	0.0304	0.002	0.0607	0.00098	0.807	0.02	0.0964	0.0017	0.76015	606	31	619	35	600	11	593	10	1.17
d_97	44.7	271.0	159.9	37000	5.34	0.15	0.0293	0.001	0.0596	0.0012	0.793	0.022	0.0964	0.0017	0.69011	583	28	580	42	592	12	593	10	-0.17
d_98	60.5	255.6	89.0	1000	10.76	0.96	0.0725	0.004	0.0905	0.0013	3.01	0.066	0.2391	0.0038	0.75618	1415	68	1431	28	1408	17	1381	20	1.92
e_121	93.0	276.0	351.0	19000	2.59	0.11	0.0286	0.002	0.063	0.0014	0.764	0.018	0.0883	0.0015	0.43704	569	29	696	48	576	10	545.1	8.7	5.36
e_123	386.0	920.0	512.0	170000	6.41	0.13	0.0806	0.004	0.1017	0.0011	3.999	0.075	0.2839	0.0042	0.81749	1567	69	1653	20	1633	15	1610	21	1.41
e_124	416.0	1538.0	712.0	26500	8.3	0.71	0.0579	0.004	0.1067	0.0019	3.604	0.097	0.2441	0.0071	0.80049	1136	69	1741	33	1549	21	1407	37	9.17
e_125	46.9	82.1	64.9	21500	4.624	0.099	0.0781	0.004	0.0945	0.0014	3.644	0.074	0.2786	0.0039	0.68397	1520	69	1512	28	1558	16	1583	19	-1.60
e_127	126.1	622.0	459.0	18000	4.04	0.16	0.0282	0.002	0.0629	0.0025	0.805	0.044	0.0923	0.003	0.69355	562	42	691	81	598	24	569	18	4.85
e_130	32.8	173.0	123.5	12500	4.53	0.12	0.0286	0.001	0.058	0.0011	0.712	0.016	0.0889	0.0012	0.53984	569	28	522	44	545.4	9.2	548.9	7.4	-0.64
e_133	405.0	954.0	536.0	153000	6.31	0.26	0.0801	0.004	0.0955	0.001	3.676	0.074	0.2778	0.0039	0.87171	1557	68	1538	21	1565	16	1580	20	-0.96
e_136	33.0	228.0	130.8	16800	5.97	0.13	0.0272	0.001	0.0615	0.00094	0.771	0.015	0.09078	0.00097	0.62255	542	26	652	32	580	8.8	560.1	5.7	3.43
e_138	170.0	472.0	233.0	24100	6.69	0.27	0.0789	0.005	0.0974	0.0016	3.536	0.081	0.263	0.0051	0.71017	1547	81	1577	28	1534	18	1504	26	1.96
e_139	65.2	256.0	242.0	15900	3.472	0.089	0.0289	0.001	0.059	0.0012	0.761	0.019	0.0934	0.0014	0.58033	576	27	563	42	573.8	11	575.5	8.2	-0.30
e_140	194.0	766.0	708.0	54000	3.65	0.14	0.0292	0.001	0.0592	0.00065	0.7639	0.014	0.0933	0.0011	0.81983	581.7	26	574	25	576	8	574.9	6.3	0.19
e_142	73.7	234.2	280.0	12100	2.8	0.12	0.0284	0.001	0.0601	0.0013	0.791	0.018	0.0951	0.0014	0.39802	566	27	598	45	591	10	587	9.1	0.68
e_144	53.0	169.0	223.0	9000	2.87	0.15	0.0267	0.001	0.0651	0.0021	0.773	0.026	0.08619	0.00099	0.28819	533	28	761	70	580	15	532.9	5.8	8.12
e_147	25.9	96.5	101.3	5600	3.34	0.1	0.0276	0.001	0.0612	0.0016	0.77	0.021	0.0913	0.0011	0.31265	551	27	622	57	579	12	563.2	6.5	2.73
e_148	120.1	388.6	477.0	900	2.93	0.14	0.0276	0.001	0.0619	0.0015	0.757	0.021	0.08842	0.00086	0.51321	550	26	664	53	572	12	546.2	5.1	4.51
e_149	181.0	501.0	685.0	10200	2.595	0.092	0.0285	0.001	0.0664	0.0012	0.857	0.019	0.0933	0.0011	0.58136	568.2	26	809	39	627.8	10	574.8	6.4	8.44
f_151	28.7	205.4	110.2	400	5.85	0.3	0.0273	0.002	0.0667	0.0025	0.816	0.038	0.0884	0.0019	0.61232	545	31	808	79	604	21	546	11	9.60
f_152	100.0	504.0	167.7	157000	10.64	0.15	0.0648	0.003	0.0815	0.00076	2.483	0.04	0.2206	0.002	0.87192	1268	57	1230	18	1267.6	12	1286.3	10	-1.48
f_153	248.0	690.0	344.0	24700	6.95	0.14	0.0782	0.004	0.0986	0.0011	3.553	0.062	0.2603	0.0026	0.80297	1521	69	1596	21	1538.3	14	1491	13	3.07
f_154	135.0	443.0	524.0	63000	3.3	0.21	0.0286	0.001	0.0621	0.0009	0.812	0.016	0.0947	0.001	0.69574	569	28	669	31	603.3	8.9	583.2	6	3.33
f_155	67.2	240.1	263.0	42000	3.25	0.12	0.0275	0.001	0.0601	0.0011	0.771	0.017	0.0927	0.0011	0.55799	548.4	26	598	40	579.5	10	571.5	6.7	1.38
f_156	65.5	277.4	244.2	37000	3.91	0.1	0.0296	0.001	0.0608	0.0013	0.785	0.02	0.0931	0.0012	0.5452	590	28	623	48	587.8	11	573.6	6.8	2.42
f_157	65.1	188.0	84.5	27000	7.97	0.81	0.084	0.004	0.0988	0.0014	3.8	0.077	0.2776	0.0041	0.71496	1630	77	1597	25	1591	16	1578	21	0.82

Appendix A. Continued.

Analysis Identifier (NB313)	Pb[1]	U[1] (ppm)	Th[1]	Isotope Ratios[2]												Ages (Ma)[3]									
				$^{206}Pb/^{204}Pb$	$^{208}Pb/^{206}Pb$	$\pm 2\sigma^2$	$^{208}Pb/^{232}Th$	$\pm 2\sigma^2$	$^{207}Pb/^{206}Pb$	$\pm 2\sigma^2$	$^{207}Pb/^{235}U$	$\pm 2\sigma^2$	$^{206}Pb/^{238}U$	$\pm 2\sigma^2$	Rho[3]	$^{208}Pb/^{232}Th$	$\pm 2\sigma^2$	$^{207}Pb/^{206}Pb$	$\pm 2\sigma^2$	$^{207}Pb/^{235}U$	$\pm 2\sigma^2$	$^{206}Pb/^{238}U$	$\pm 2\sigma^2$	% disc.[4]
f_158	98.2	282.0	387.0	88000	2.598	0.067	0.0277	0.001	0.0581	0.001	0.749	0.016	0.0932	0.0011	0.59312	552	26	523	38	566.8	9.4	574.3	6.2	-1.32
f_160	60.6	246.0	241.0	44000	3.471	0.093	0.0268	0.001	0.0623	0.0019	0.785	0.027	0.0911	0.0015	0.46265	534	25	668	65	587	15	561.8	9	4.29
f_161	48.8	199.0	184.0	1E+06	3.63	0.088	0.0289	0.002	0.0608	0.0016	0.786	0.022	0.0936	0.0013	0.36503	576	29	612	56	588	12	576.5	7.9	1.96
f_163	144.6	392.0	573.0	710000	2.289	0.065	0.026	0.001	0.0602	0.0017	0.772	0.026	0.0928	0.0022	0.56288	520	26	601	60	580	15	572	13	1.38
f_164	36.9	52.3	23.9	170000	7.97	0.23	0.1686	0.009	0.2078	0.003	17.1	0.37	0.5944	0.0082	0.75389	3146	150	2885	23	2939	21	3006	33	-2.28
f_166	87.6	357.0	313.0	590000	3.99	0.24	0.0311	0.002	0.0646	0.0019	0.821	0.023	0.0926	0.0014	0.17512	618	30	749	60	608	13	570.7	8.5	6.13
f_168	133.7	475.0	218.0	870000	7.8	0.28	0.0663	0.003	0.0857	0.0012	2.696	0.055	0.2275	0.0031	0.72989	1297	60	1327	27	1326	15	1321	16	0.38
f_169	93.6	1092.0	96.3	46500	30.8	1.2	0.1021	0.006	0.0972	0.0013	3.497	0.059	0.2594	0.0028	0.6103	1964	99	1566	24	1527.1	14	1486	14	2.69
f_173	16.2	52.4	21.7	52000	8.25	0.28	0.0808	0.004	0.0942	0.0019	3.329	0.078	0.2569	0.0036	0.51553	1569	81	1500	38	1487	19	1473	18	0.94
f_174	134.0	387.0	148.4	5100	8.39	0.67	0.099	0.005	0.1201	0.0019	5.332	0.12	0.3219	0.0039	0.73902	1908	90	1953	27	1872	19	1798	19	3.95
f_175	101.7	362.0	391.0	51000	3.205	0.096	0.0282	0.001	0.0622	0.0012	0.791	0.018	0.0921	0.0012	0.53187	561	26	679	40	591.1	10	567.6	7.2	3.98
f_176	70.8	273.9	276.9	48000	3.465	0.081	0.0277	0.001	0.0603	0.0012	0.772	0.017	0.0925	0.0012	0.45013	551.9	25	603	43	580	10	570.3	7	1.67
f_178	43.0	225.0	156.7	25000	4.63	0.1	0.0296	0.001	0.0634	0.0014	0.81	0.018	0.0927	0.0013	0.3255	589	28	709	46	602.1	10	571.5	7.5	5.08
f_180	211.0	620.0	799.0	34000	2.82	0.22	0.0296	0.002	0.0634	0.0014	0.805	0.021	0.0926	0.0018	0.56279	588	29	712	46	599	12	571	10	4.67
Excluded analyses, <10% precision and/or >10% discordant																									
a_04	141.4	333.0	278.0	426	2.173	0.04	0.0529	0.003	0.1351	0.0018	1.935	0.042	0.103	0.0013	0.82662	1042	49	2162	23	1092	14	631.7	7.7	42.15
a_05	367.0	1069.0	1114.0	892	2.298	0.058	0.033	0.002	0.0956	0.0022	1.206	0.034	0.0908	0.0014	0.57854	657	33	1534	45	802	16	560.2	8.5	30.15
a_06	239.0	543.0	376.0	606	2.625	0.097	0.0668	0.004	0.1189	0.0041	2.005	0.074	0.1213	0.0016	0.3565	1307	66	1925	61	1114	25	738	9.4	33.75
a_08	31.4	115.7	95.4	770	3.21	0.1	0.0336	0.002	0.0734	0.0021	0.962	0.031	0.0943	0.0014	0.46015	668	34	1013	60	685	17	581	8.1	15.18
a_20	106.2	385.0	379.0	3710	2.894	0.075	0.0296	0.001	0.0786	0.0027	0.967	0.038	0.089	0.0017	0.48566	589	28	1163	67	685	19	549	10	19.85
a_22	155.0	629.0	492.0	8600	3.463	0.097	0.0323	0.002	0.0702	0.0011	0.941	0.025	0.0964	0.0015	0.84923	643	30	942	36	673	13	593.4	8.8	11.83
a_27	123.3	192.8	101.4	3420	3.73	0.15	0.1231	0.007	0.1254	0.0028	4.67	0.13	0.2691	0.0045	0.59719	2344	130	2027	40	1759	23	1536	23	12.68
b_35	115.2	248.0	117.0	842	1.993	0.059	0.118	0.012	0.2041	0.0058	2.75	0.11	0.0971	0.0014	0.86725	2240	210	2846	46	1336	28	597.5	8	55.28
b_37	39.7	211.0	124.0	23000	5.18	0.23	0.0333	0.002	0.0695	0.0019	0.895	0.027	0.0937	0.0012	0.42283	662	47	904	53	648	14	577.3	7.3	10.91
b_43	65.7	359.0	206.9	4300	4.71	0.14	0.0327	0.002	0.0714	0.0014	0.955	0.026	0.0973	0.0017	0.69586	650	30	959	40	679	13	598	10	11.93
b_54	93.8	375.0	323.0	25000	3.33	0.12	0.0299	0.002	0.0708	0.0019	0.91	0.027	0.0938	0.0013	0.42828	595	30	940	54	656	14	578.2	7.4	11.86
c_69	125.6	663.0	390.2	24100	4.485	0.059	0.0343	0.002	0.0798	0.0011	1.003	0.021	0.0914	0.0011	0.78012	682.4	31	1188	27	704.8	11	563.5	6.7	20.05

Appendix A. Continued.

Analysis Identifier (NB313)	Pb[1]	U[1] (ppm)	Th[1]	Isotope Ratios[2]												Ages (Ma)[3]									
				$^{206}Pb/^{204}Pb$	$^{208}Pb/^{206}Pb$	± 2σ[2]	$^{208}Pb/^{232}Th$	± 2σ[2]	$^{207}Pb/^{206}Pb$	± 2σ[2]	$^{207}Pb/^{235}U$	± 2σ[2]	$^{206}Pb/^{238}U$	± 2σ[2]	Rho[3]	$^{208}Pb/^{232}Th$	± 2σ[2]	$^{207}Pb/^{206}Pb$	± 2σ[2]	$^{207}Pb/^{235}U$	± 2σ[2]	$^{206}Pb/^{238}U$	± 2σ[2]	% disc.[4]
c_70	142.6	895.0	485.0	43700	5.13	0.14	0.0307	0.001	0.0704	0.001	0.856	0.017	0.0884	0.0012	0.69905	610	28	935	30	627.2	9.5	546.1	7	12.93
c_74	58.6	209.2	139.4	21300	3.17	0.13	0.0429	0.003	0.1011	0.004	1.375	0.067	0.0989	0.0021	0.60882	848	48	1628	73	875	28	608	13	30.51
c_76	85.0	128.0	103.5	25700	3.82	0.12	0.0864	0.004	0.1282	0.0031	4.896	0.093	0.2788	0.0047	0.09413	1674	77	2067	42	1801	16	1585	23	11.99
c_77	63.5	135.3	123.1	5210	1.81	0.048	0.0526	0.003	0.1819	0.004	2.368	0.066	0.0948	0.0016	0.61449	1035	51	2664	37	1231	20	583.9	9.3	52.57
c_78	79.9	318.0	272.0	21200	3.33	0.13	0.0315	0.002	0.0972	0.0033	1.227	0.042	0.0919	0.0011	0.19807	626	41	1577	68	817	21	566.7	6.3	30.64
c_79	77.2	236.7	251.0	41000	2.47	0.12	0.0304	0.002	0.071	0.0027	0.906	0.041	0.0929	0.0023	0.5421	605	30	946	82	654	22	573	14	12.39
c_83	92.6	485.0	250.0	93000	4.76	0.11	0.0382	0.002	0.0745	0.0021	1.063	0.03	0.1048	0.0017	0.28949	758	40	1041	52	737	16	642	10	12.89
c_85	91.7	371.0	305.0	134000	3.54	0.11	0.0323	0.002	0.073	0.0016	0.936	0.027	0.0931	0.0012	0.69639	641	31	1006	43	669	14	573.8	6.9	14.23
c_88	723.0	1149.0	2280.0	143000	1.81	0.18	0.0367	0.002	0.0763	0.0013	1.055	0.025	0.1006	0.0013	0.71555	729	47	1096	33	730	12	617.8	7.5	15.37
c_90	133.0	286.0	546.0	140000	1.807	0.089	0.0263	0.001	0.0678	0.0015	0.827	0.02	0.0887	0.0015	0.46625	524	25	868	40	611.6	11	547.6	9	10.46
d_103	75.3	195.0	179.5	5710	2.234	0.092	0.0438	0.003	0.1356	0.0055	1.763	0.079	0.095	0.0016	0.42828	865	49	2147	68	1027	28	584.8	9.3	43.06
d_105	399.0	726.0	1482.0	22500	1.542	0.021	0.0286	0.001	0.0778	0.0012	0.995	0.018	0.09309	0.00089	0.52258	569	26	1135	30	700.7	9.4	573.7	5.2	18.12
d_114	87.3	350.1	315.9	30000	3.26	0.12	0.0279	0.002	0.0728	0.0029	0.917	0.036	0.0921	0.0023	0.29479	556	30	993	82	660	19	568	14	13.94
d_115	60.1	256.0	176.0	11900	3.57	0.11	0.0352	0.002	0.0867	0.0024	1.163	0.052	0.0977	0.0029	0.79641	698	40	1345	54	781	25	600	17	23.18
d_120	36.6	116.6	129.3	2100	2.722	0.082	0.0303	0.002	0.0809	0.003	0.997	0.041	0.0899	0.0016	0.43227	603	31	1198	75	700	21	554.6	9.6	20.77
d_92	22.2	68.3	75.0	40000	2.81	0.092	0.0323	0.002	0.075	0.0037	0.955	0.046	0.092	0.0016	0.11268	643	35	1070	110	685	27	567.6	9.7	17.14
d_93	138.9	342.8	410.0	10300	2.093	0.053	0.0359	0.002	0.1227	0.0032	1.582	0.05	0.0933	0.0013	0.58234	712	38	1989	46	962	20	575.2	7.9	40.21
d_99	307.0	678.0	1100.0	53000	2.15	0.17	0.0299	0.001	0.0706	0.0012	0.989	0.025	0.1014	0.0016	0.75095	595	28	939	36	697	13	622.5	9.2	10.69
e_122	451.0	2141.0	1640.0	7200	3.55	0.21	0.0308	0.003	0.0844	0.0047	0.933	0.069	0.079	0.0021	0.78206	612	48	1251	96	661	33	490	12	25.87
e_126	140.0	321.0	588.0	5800	1.761	0.024	0.0255	0.001	0.0794	0.0013	0.885	0.021	0.07987	0.00081	0.82661	508.6	23	1183	33	642.5	11	495.3	4.9	22.91
e_128	104.4	344.1	291.0	5600	3.03	0.11	0.0377	0.002	0.0913	0.0052	1.263	0.081	0.0982	0.0018	0.51259	748	43	1440	110	821	34	604	11	26.43
e_129	130.0	105.5	142.0	492	1.011	0.037	0.1008	0.007	0.348	0.012	5.94	0.32	0.1229	0.0034	0.8315	1939	120	3702	57	1959	44	747	20	61.87
e_131	60.8	168.5	228.0	2000	2.331	0.095	0.0293	0.002	0.0871	0.0039	1.021	0.055	0.0845	0.0011	0.76036	584	32	1307	89	711	28	523	6.7	26.44
e_132	110.7	200.0	207.0	928	1.775	0.044	0.0565	0.003	0.1837	0.0051	2.684	0.091	0.1056	0.0016	0.5921	1111	58	2676	45	1321	25	647	9.6	51.02
e_134	74.3	301.0	196.5	6100	4.08	0.11	0.0409	0.002	0.085	0.0018	1.247	0.03	0.1062	0.0018	0.51208	809	39	1309	41	821	14	651	11	20.71
e_135	52.0	157.0	168.0	1000	2.879	0.077	0.0347	0.002	0.0793	0.0015	1.056	0.023	0.0957	0.0012	0.5013	688	34	1178	41	731.2	11	588.9	6.9	19.46
e_137	111.6	394.0	282.0	2120	3.123	0.07	0.0427	0.003	0.1048	0.0024	1.403	0.037	0.09691	0.00099	0.51112	844	50	1712	45	889	16	596.2	5.8	32.94
e_141	74.4	275.4	214.1	2620	3.31	0.14	0.0383	0.002	0.0987	0.0016	1.282	0.027	0.094	0.0011	0.64456	759	43	1594	31	836.9	12	579.1	6.2	30.80

Appendix A. Continued.

Analysis Identifier (NB313)	Pb[1]	U[1] (ppm)	Th[1]	Isotope Ratios[2]												Ages (Ma)[3]									
				$^{206}Pb/^{204}Pb$	$^{208}Pb/^{206}Pb$	± 2σ[2]	$^{208}Pb/^{232}Th$	± 2σ[2]	$^{207}Pb/^{206}Pb$	± 2σ[2]	$^{207}Pb/^{235}U$	± 2σ[2]	$^{206}Pb/^{238}U$	± 2σ[2]	Rho[3]	$^{208}Pb/^{232}Th$	± 2σ[2]	$^{207}Pb/^{206}Pb$	± 2σ[2]	$^{207}Pb/^{235}U$	± 2σ[2]	$^{206}Pb/^{238}U$	± 2σ[2]	% disc.[4]
e_143	167.0	203.4	750.0	1800	1.46	0.13	0.0271	0.002	0.0709	0.0018	0.994	0.028	0.1015	0.0017	0.45514	541	36	946	51	700	14	622.8	9.7	11.03
e_145	29.8	118.6	106.2	300	3.69	0.17	0.0302	0.002	0.0719	0.0019	0.977	0.029	0.0981	0.0013	0.45553	601	31	970	54	691	15	603.1	7.8	12.72
e_146	70.0	174.1	149.9	1050	2.266	0.065	0.0497	0.003	0.1405	0.0036	1.923	0.052	0.0992	0.0015	0.37093	981	54	2238	49	1093	20	609.7	8.9	44.22
e_150	139.1	416.0	368.0	1490	2.62	0.25	0.0388	0.003	0.1099	0.0043	1.504	0.067	0.0992	0.0031	0.51367	768	51	1788	71	930	27	610	18	34.41
f_159	371.0	779.0	1230.0	11400	2.091	0.066	0.0332	0.002	0.0716	0.0014	1.008	0.028	0.1013	0.0016	0.72794	660	32	974	41	707	14	622	9.4	12.02
f_167	95.0	267.0	330.0	58000	2.78	0.2	0.0327	0.002	0.0783	0.0017	1.068	0.036	0.0978	0.0019	0.79579	650	42	1159	48	736	17	602	11	18.21
f_170	122.0	298.1	430.0	5100	2.226	0.057	0.0308	0.002	0.0839	0.0019	1.114	0.032	0.0964	0.0015	0.6202	612	29	1291	46	762	17	593.4	8.9	22.13
f_171	45.2	117.0	48.4	1030	3.94	0.23	0.1004	0.006	0.1242	0.0045	2.843	0.1	0.1666	0.0051	0.40008	1933	100	1998	62	1363	27	993	28	27.15
f_172	224.0	1328.0	882.0	5600	5.59	0.16	0.0284	0.002	0.0707	0.0015	0.92	0.027	0.0952	0.0018	0.69261	566	29	941	42	665	15	586	10	11.88
f_177	122.0	1100.0	207.0	3900	11.7	1.2	0.071	0.012	0.0828	0.0035	1.668	0.061	0.1457	0.0049	0.27712	1390	220	1254	77	995	22	877	28	11.86
f_179	73.5	206.0	206.0	920	2.623	0.087	0.0392	0.002	0.1001	0.003	1.329	0.045	0.0968	0.0014	0.46708	778	42	1611	53	856	19	595.5	8.1	30.43
f_151	28.7	205.4	110.2	400	5.85	0.3	0.0273	0.002	0.0667	0.0025	0.816	0.038	0.0884	0.0019	0.61232	545	31	808	79	604	21	546	11	9.60
d_103	75.3	195.0	179.5	5710	2.234	0.092	0.0438	0.003	0.1356	0.0055	1.763	0.079	0.095	0.0016	0.42828	865	49	2147	68	1027	28	584.8	9.3	43.06
d_114	87.3	350.1	315.9	30000	3.26	0.12	0.0279	0.002	0.0728	0.0029	0.917	0.036	0.0921	0.0023	0.29479	556	30	993	82	660	19	568	14	13.94
d_120	36.6	116.6	129.3	2100	2.722	0.082	0.0303	0.002	0.0809	0.003	0.997	0.041	0.0899	0.0016	0.43227	603	31	1198	75	700	21	554.6	9.6	20.77
e_122	451.0	2141.0	1640.0	7200	3.55	0.21	0.0308	0.003	0.0844	0.0047	0.933	0.069	0.079	0.0021	0.78206	612	48	1251	96	661	33	490	12	25.87
e_141	74.4	275.4	214.1	2620	3.31	0.14	0.0383	0.002	0.0987	0.0016	1.282	0.027	0.094	0.0011	0.64456	759	43	1594	31	836.9	12	579.1	6.2	30.80
Primary reference material[5]																									
91500 (n=87	15.2	84.9	29.7	46793	9.358	0.336	0.0542	0.003	0.0749	0.00174	1.851	0.05	0.17932	0.00297	0.52548	1062.6	12.4	1053.6	9.0	1063.5	3.7	1064.7	3.2	
Secondary reference material(s)[5]																									
FC1 (n=49)	240.6	696.5	446.5	4E+06	5.573	0.107	0.057	0.003	0.0766	0.00114	2.0129	0.042	0.1906	0.00266	0.69378	1119.6	7.5	1100.0	5.3	1116.7	1.9	1119.5	1.8	
R33 (n=28)	33.7	243.2	175.8	49260	4.96	0.14	0.0206	0.001	0.0561	0.00117	0.5236	0.013	0.06768	0.00073	0.49626	410.7	3.9	443.0	16.1	426.0	1.5	421.6	0.8	

[1] U-Th-Pb concentrations referenced to either NIST 612 glass or 91500 zircon; concentration uncertainty approximately ± 20%. [2] Isotope ratios not corrected for common Pb.

[3] Dates calculated with decay constants of Jaffey *et al*. (1971) and 238U/235U = 137.818 (Hiess, 2012) using Iolite v. 3.5 (Paton *et al*. 2011) and U-Pb Geochron4 DRS (Paton *et al*. 2010).

Preferred dates used in plots are $^{206}/^{238}$ dates less than 700 Ma and 207/206 dates greater than 700 Ma. [4] Discordance calculated as (1-($^{206}Pb/^{238}U$ age / $^{207}Pb/^{235}U$ age))*100.

[5] Concentration data are means of all anlayses; dates and isotope ratios are weighted means of all analyses <2% discordant. Average reproducibility of individual U–Pb dates from primary reference material is better than 0.7% (reduced separately as unknowns) and average accuracy of secondary reference material is better than 2.25% (FC-1) and better than 1.5% (R33).

Appendix B. Major and trace element chemical data for mafic and intermediate volcanic rocks in the Almond Road and Belleisle Bay groups.

Sample	10SJ-10	10SJ-15	1630225	1630322	06SJ-057	10SJ-11	10SJ-34	10SJ-37	10SJ-38	10SJ-41	10SJ-16	10SJ-18	10SJ-19	10SJ-21
Unit	Almond Rd. Group				Browns Flat Fm.						Grant Brook Fm			
Zone	20	20	19	19	20	20	20	20	20	20	20	20	20	20
Easting	266888	275060	732153	733116	280351	269501	294433	288534	288574	270126	297403	297325	297275	297181
Northing	5055869	5061551	5054959	5055170	5062935	5055154	5076280	5071884	5071840	5053942	5080347	5080680	5080855	5081009
SiO_2	50.29	53.97	49.11	47.79	48.05	50.40	52.52	48.62	52.20	49.24	55.43	50.18	48.37	61.23
TiO_2	1.15	1.07	1.66	0.82	2.31	2.76	1.04	0.65	1.29	0.65	1.85	1.64	0.95	1.30
Al_2O_3	16.61	17.93	18.69	18.01	13.97	13.06	15.36	15.30	18.64	17.67	19.92	20.59	17.71	14.98
Fe_2O_3[1]	9.47	6.88	11.80	9.57	12.19	13.30	8.51	8.38	11.18	9.45	5.68	10.30	9.89	6.71
MnO	0.14	0.10	0.18	0.13	0.23	0.19	0.14	0.14	0.15	0.18	0.12	0.16	0.28	0.30
MgO	6.18	3.48	5.26	5.25	4.91	3.65	6.73	11.01	4.80	8.46	1.43	2.45	6.68	3.16
CaO	4.71	2.43	3.54	8.01	8.21	4.09	6.57	8.14	1.45	4.15	2.48	6.09	4.65	3.50
Na_2O	5.40	7.36	5.02	4.97	3.61	4.64	2.95	2.39	4.72	4.49	6.56	3.48	4.31	1.46
K_2O	0.27	0.06	1.09	0.05	0.74	0.10	0.17	0.14	0.55	0.07	2.09	1.31	1.62	2.97
P_2O_5	0.16	0.23	0.22	0.21	0.35	1.42	0.21	0.07	0.16	0.08	0.72	0.35	0.16	0.38
Cr	80	10	10	180	50	10	280	790	70	60	10	70	220	10
Ni	50	10	10	80	30	10	150	260	40	50	10	50	70	10
Co	31	19	34	36	31	14	36	46	35	37	10	36	46	12
Sc	30	16	29	38	38	34	26	37	36	32	25	27	36	17
V	231	130	262	239	357	116	183	221	305	219	99	142	219	102
Cu	50	40	40	70	40	10	40	50	130	110	5	10	90	5
Pb	2.5	7	2.5	2.5	2.5	8	7	2.5	2.5	2.5	16	12	5	14
Zn	50	100	80	60	100	90	50	50	70	70	100	100	60	70
Ga	15	16	19	15	20	20	15	13	19	15	26	19	21	20
Cs	0.5	0.8	0.25	0.25	0.25	0.3	0.4	3	2.5	2.8	2.2	1	2.7	6.2
Rb	3	0.5	9	1	14	3	4	3	13	1	76	37	58	96
Ba	95	144	572	41	265	1105	107	147	194	51	461	286	454	653
Sr	149	281	341	111	486	282	976	178	330	280	538	270	319	274
Ta	0.2	0.24	0.3	0.1	0.4	0.52	0.61	0.07	0.27	0.06	1.2	0.58	0.21	0.81
Nb	2.3	4	3	1	6	6.3	8.4	1.3	3.8	0.8	17.5	7.9	3.1	11.7
Hf	2.1	4.2	3.6	1.6	4.1	3.1	2.8	1.3	2.8	1.1	8.9	4.1	1.8	5.7
Zr	92	196	131	50	151	136	131	49	118	39	428	198	80	276
Y	21.4	33.2	31	21	42	48.6	16.8	15.7	24.3	10.7	59.5	29.4	16.7	38.3
Th	1.34	2.76	1.2	0.7	1.7	2.93	3.64	0.77	2.07	0.37	12.8	5.69	2.17	8.7
U	0.39	0.59	0.8	0.3	0.5	0.74	0.92	0.17	0.39	0.09	2.33	1.47	0.47	2.18
La	6.14	12.00	9.90	4.90	13.30	21.40	19.80	3.75	9.00	3.04	72.20	28.40	12.70	41.90
Ce	14.70	30.60	25.40	11.80	31.90	50.90	42.20	7.79	20.30	7.66	162.00	67.00	24.90	92.90
Pr	2.05	4.17	3.80	1.69	4.62	7.25	4.90	1.10	2.58	1.08	19.80	8.74	3.08	11.40
Nd	9.89	19.00	18.40	8.60	22.20	36.20	20.30	5.68	12.10	5.76	81.10	38.00	14.20	46.30
Sm	3.10	4.95	4.90	2.50	6.10	9.76	4.29	1.70	3.45	1.61	17.00	8.67	3.50	10.10
Eu	0.99	1.40	1.79	0.95	2.21	3.75	1.27	0.65	1.01	0.58	4.46	2.23	1.08	2.66
Gd	3.51	5.21	5.30	3.00	7.00	10.70	3.69	2.19	3.56	1.78	13.90	7.02	3.67	8.46
Tb	0.65	0.91	0.90	0.60	1.20	1.72	0.56	0.41	0.70	0.33	2.07	1.09	0.57	1.27
Dy	3.84	5.87	5.70	3.70	7.90	9.90	3.46	2.86	4.38	2.09	11.20	6.05	3.31	7.21
Ho	0.81	1.20	1.10	0.80	1.60	1.93	0.68	0.61	0.92	0.42	2.20	1.12	0.65	1.39
Er	2.32	3.55	3.40	2.30	4.60	5.36	1.97	1.79	2.91	1.22	6.15	3.19	1.96	3.94
Tm	0.34	0.56	0.50	0.34	0.67	0.76	0.29	0.28	0.46	0.18	0.87	0.45	0.29	0.57
Yb	2.17	3.80	3.20	2.10	4.30	4.54	1.76	1.87	3.00	1.25	5.71	2.77	1.92	3.75
Lu	0.36	0.62	0.47	0.32	0.64	0.72	0.30	0.29	0.49	0.21	0.89	0.45	0.30	0.59
Zr/Y	4.30	5.90	4.23	2.38	3.60	2.80	7.80	3.12	4.86	3.64	7.19	6.73	4.79	7.21
Th/Yb	0.62	0.73	0.38	0.33	0.40	0.65	2.07	0.41	0.69	0.30	2.24	2.05	1.13	2.32

Appendix B. Continued.

Sample	10SJ-23	10SJ-33	10SJ-39	NB07-02	06SJ-044	06SJ-063	10SJ-33A	10SJ-40
Unit	Grant Brook Fm							
Zone	20	20	20	20	20	20	20	20
Easting	297048	288829	288779	275706	297196	289023	288829	290201
Northing	5081255	5071219	5071391	5061120	5079767	5073595	5071219	5074627
SiO_2	49.66	47.08	50.96	63.21	65.11	56.95	68.61	61.24
TiO_2	1.07	2.62	0.82	0.79	1.34	0.96	0.59	0.40
Al_2O_3	18.27	15.49	17.24	16.03	14.78	16.39	14.62	17.54
Fe_2O_3[1]	10.39	13.62	8.25	6.80	6.81	7.91	3.72	5.13
MnO	0.22	0.20	0.13	0.20	0.08	0.13	0.06	0.15
MgO	6.84	4.19	5.39	1.70	1.94	4.76	0.77	1.32
CaO	5.70	5.30	3.84	1.35	1.25	2.86	2.25	1.34
Na_2O	3.17	4.51	6.15	4.28	6.27	5.45	4.46	8.18
K_2O	0.22	0.16	0.26	1.19	0.56	0.16	1.69	0.07
P_2O_5	0.15	0.36	0.23	0.17	0.60	0.19	0.17	0.19
Cr	100	50	90	30	10	50	10	10
Ni	60	30	40	20	10	40	10	10
Co	46	37	30	17	8	26	5	4
Sc	35	39	23	20	17	28	9	6
V	286	361	178	141	83	182	31	18
Cu	60	50	40	40	10	90	5	5
Pb	13	7	10	14	19	12	5	2.5
Zn	60	130	50	80	80	60	15	15
Ga	19	22	18	18	15	15	18	13
Cs	0.5	1	2.4	4.2	0.25	3.5	3.1	0.4
Rb	5	4	10	46	19	6	55	0.5
Ba	151	89	214	221	142	141	222	29
Sr	602	169	734	219	217	445	102	108
Ta	0.16	0.54	0.36	0.55	0.8	0.4	0.79	0.16
Nb	2.9	7.3	4.7	6.5	11	5	8.6	2.6
Hf	2.4	4.5	3.5	3.7	6.8	3.9	5.3	2.3
Zr	105	192	147	164	252	136	253	112
Y	26	35.2	22.7	25	40	25	31.5	21.1
Th	3.43	2.03	5.64	6.58	8.8	7.1	7.34	1.36
U	0.98	0.54	1.25	1.44	1.8	1.6	1.35	0.43
La	16.80	13.00	22.80	24.50	36.70	30.40	26.40	7.62
Ce	38.10	32.10	51.00	51.70	70.60	68.30	55.90	18.30
Pr	5.12	4.27	6.24	6.20	10.20	7.92	6.33	2.52
Nd	22.80	20.60	26.50	25.70	44.40	33.80	25.50	11.40
Sm	5.21	5.78	5.50	5.74	9.50	7.00	5.57	3.09
Eu	1.44	1.63	1.38	1.34	2.42	1.97	1.26	0.88
Gd	4.88	6.14	4.61	5.01	8.50	5.90	5.14	3.25
Tb	0.82	1.10	0.72	0.79	1.40	1.00	0.91	0.56
Dy	4.74	6.82	4.22	4.65	8.20	5.40	5.66	3.43
Ho	0.94	1.39	0.87	0.91	1.60	1.00	1.16	0.74
Er	2.78	4.19	2.51	2.78	4.60	2.90	3.56	2.24
Tm	0.40	0.65	0.38	0.42	0.66	0.42	0.55	0.36
Yb	2.59	4.40	2.54	2.85	4.20	2.70	3.79	2.58
Lu	0.41	0.71	0.42	0.49	0.62	0.39	0.63	0.45
Zr/Y	4.04	5.45	6.48	6.56	6.30	5.44	8.03	5.31
Th/Yb	1.32	0.46	2.22	2.31	2.10	2.63	1.94	0.53